

Replies to the Editor comments

1. I have read the revised version of your work as well as the answers you provided to my comments. I find the manuscript much improved but I still have comments.

I have problems with the title, “Optimization of Biological Production for Indian Ocean upwelling zones: Part – I: Improving Biological Parameterization via a variable Compensation Depth” because the paper is not dealing with optimization of biological production (better estimation but not optimization). I would suggest something like “Biological production in the Indian Ocean upwelling zones: Part –I: refined estimation via the use of a variable compensation depth in ocean carbon models. “ it would more reflect the content of your paper.

Thank you for your suggestion. We agree that the word ‘optimization’ may be bit confusing in this context, and we accept the title suggested by the Editor. As per your advice we are restating the title of our paper as “Biological production in the Indian Ocean upwelling zones: Part-I: refined estimation via the use of a variable compensation depth in ocean carbon models”.

2. I also find that the paper is very long with notably 8 tables and 21 figures which may render difficult to capture the main messages. I would suggest that you consider to put some figures as supplements and that you leave in the main text the most striking ones.

Thank you for your suggestion. In fact it is true that the number of figures are quiet large. We have decided to move Tables 7, 8, Figures 16 to 21 and relevant text (of the sensitivity experiments from section 4) to supplementary material.

3. In your answer to my comments, you mentioned that biological production will be defined in the text (you mentioned lines 729-730) but it is not the case. So please define biological production since the beginning (Introduction). For instance (Lines 123-), when

you defined Z_c , it will be appropriate that you inform the reader on what will be the biological production in this manuscript.

As per the Editor's comment we have explicitly stated the above lines (i.e. 729-730) in the Introduction part immediately after defining Z_c . The revised line numbers are 109 - 114.

4. Lines 154-155 : Please reformulate.

Reformulated as “The improvements due to the effect of a variable Z_c over the Indian Ocean and the sensitivity experiments where upwelling is muted strongly imply that the biological pump may play as much of a role as the solubility pump in determining surface $p\text{CO}_2$ and CO_2 fluxes over the Indian Ocean”. Please refer lines 143 – 146 in the revised manuscript.

5. Line 221-223: Please refer appropriately to appendix for details on the model equations.

Citation to the Appendix is added properly to Section 2.2.

6. Line 226 : J_{prod} has to be defined.

J_{prod} represents the biogeochemical flows with respect to production of organic phosphorous.

Please refer lines 200 – 201 in the revised manuscript.

7. Lines 226-229: I suppose that $J_{prod} = (2)$ if $\text{PO}_4 > \text{PO}_4^*$ and $Z < Z_c$ While $J_{prod} = 0$ if $\text{PO}_4 < Z_c$? Please clarify as it is not clear if the two conditions are needed or not. (it is needed at line 227 while at line 229 it is one of the two if I am right)

Thank you for pointing this out. This was a typo and we appreciate your eye to the detail. This has been rectified as below.

$$J_{prod} = \frac{1}{\tau}([PO_4] - [PO_4]^*) ; \quad [PO_4] > [PO_4]^* ; \quad Z < Z_c \quad \text{Eq(1)}$$

$$J_{prod} = 0 ; \quad [PO_4] \leq [PO_4]^* \quad \text{Eq(2)}$$

Please refer equations 2 and 3 in the revised manuscript.

8. Line 283: suppresses

Corrected accordingly. Please refer lines 251 - 252 in the revised manuscript.

9. Lines 294-304: Z_c , NPP,.. have already been defined before in the introduction (lines 107-123)

Corrected accordingly, Please refer lines 264 - 268 in the revised manuscript.

10. Line 320: Why 50 W/m²? Equations (2) suggest a difference for Z

Thank you for pointing this out. Corrected as 10 W m⁻². Please refer to lines 286 – 287 in the revised manuscript.

11. Line 745: “are” the biological source/sink terms..

Corrected accordingly. Please refer to lines 638 - 639 in the revised manuscript.

12. Line 746 “ due to evaporation..” do you mean air-sea exchange?

No, We do not mean air-sea exchange. It accounts for dilution and concentration of water by precipitation and evaporation, and corresponding changes in DIC, ALK etc. They are different from the air-sea exchange term which is $J_g DIC$.

Please refer to lines 639 to 641 in the revised manuscript.

13. Lines 750-753: you use JDOP, JPO4, JDIC, JALK while above you use JbPO4, JbDOP,.. please homogenize the notation for clarity.

Corrected accordingly. Please refer to lines 637 - 639 in the revised manuscript.

14. Line 764: JDOP, ..already defined above

Corrected accordingly. Please refer to lines 653-654 in the revised manuscript.

15. Line 801 remove “is” because it is written twice.

Corrected accordingly. Please refer to line 690 in the revised manuscript.

1 **Biological Production in the Indian Ocean Upwelling Zones: Part – I: Refined Estimation**
2 **via the Use of a Variable Compensation Depth in Ocean Carbon Models**

3

4 Mohanan Geethalekshmi Sreeush^{1,2,*}.

5 Vinu Valsala¹,

6 Sreenivas Pentakota¹,

7 Koneru Venkata Siva Rama Prasad²,

8 Raghu Murtugudde³

9

10 ¹Indian Institute of Tropical Meteorology, Pune, India

11 ²Department of Meteorology and Oceanography, Andhra University, India

12 ³ESSIC, University of Maryland, USA

13

14 *(Under revision BGD)*

15

16 *Corresponding author address:

17 Indian Institute of Tropical Meteorology,

18 Dr. Homi Bhabha Road, Pashan, Pune 411 008, India

19 E-Mail: sreeushmg@tropmet.res.in

20

21 **Abstract**

22

23 Biological modeling approach adopted by the Ocean Carbon-cycle Model Inter-comparison
24 Project (OCMIP-II) provided amazingly simple but surprisingly accurate rendition of the annual
25 mean carbon cycle for the global ocean. Nonetheless, OCMIP models are known to have
26 seasonal biases which are typically attributed to their bulk parameterization of ‘compensation
27 depth’. Utilizing the criteria of surface Chl-a based attenuation of solar radiation and the
28 minimum solar radiation required for production, we have proposed a new parameterization for a
29 spatially and temporally varying ‘compensation depth’ which captures the seasonality in the
30 production zone reasonably well. This new parameterization is shown to improve the seasonality
31 of CO₂ fluxes, surface ocean pCO₂, biological export and new production in the major upwelling
32 zones of the Indian Ocean. The seasonally varying compensation depth enriches the nutrient
33 concentration in the upper ocean yielding more faithful biological exports which in turn leads to
34 an accurate seasonality in the carbon cycle. The export production strengthens by ~70% over the
35 western Arabian Sea during monsoon period and achieves a good balance between export and
36 new production in the model. This underscores the importance of having a seasonal balance in
37 model export and new productions for a better representation of the seasonality of carbon cycle
38 over upwelling regions. The study also implies that both the biological and solubility pumps play
39 an important role in the Indian Ocean upwelling zones.

40

41 Keywords: Indian Ocean upwelling zones, Carbon cycle, Seasonal cycle - CO₂ flux and Oceanic
42 pCO₂, Biogeochemical model parameterization, Export production - New production balance,
43 Solubility and Biological pump.

44

45 **1. Introduction**

46 The Indian Ocean is characterized by the unique seasonally reversing monsoon wind systems
47 which act as the major physical drivers for the coastal and open ocean upwelling processes. The
48 major upwelling systems in the Indian Ocean are (1) the western Arabian Sea (WAS; Ryther and
49 Menzel, 1965; Smith et al., 2001; Sarma, 2004; Wiggert et al., 2005, 2006; Murtugudde et al.,
50 2007; McCreary et al., 2009; Prasanna Kumar et al., 2010; Naqvi et al., 2010; Roxy et al., 2015)
51 (2) the Sri Lanka Dome (SLD; Vinayachandran et al., 1998, 2004), (3) Java and Sumatra coasts
52 (SC; Murtugudde et al., 1999; Susanto et al., 2001; Osawa et al., 2010; Xing et al., 2012) and (4)
53 the Seychelles-Chagos thermocline ridge (SCTR; Murtugudde et al., 1999; Dilmahamod et al.,
54 2016, Figure 1). The physical and biological processes and their variability over these key
55 regions are inseparably tied to the strength of the monsoon winds and associated nutrient
56 dynamics. The production and its variability over these coastal upwelling systems are a key
57 concern for the fishing community, since they affect the day-to-day livelihood of the coastal
58 populations (Harvell et al., 1999; Roxy et al., 2015; Praveen et al., 2016) and are important for
59 the Indian Ocean rim countries due to their developing country status.

60 Arabian Sea is a highly productive coastal upwelling system characterized by phytoplankton
61 blooms both in summer (Prasanna Kumar et al., 2001; Naqvi et al., 2003; Wiggert et al., 2005)
62 and winter (Banse and McClain, 1986; Wiggert et al., 2000; Barber et al., 2001; Prasannakumar
63 et al., 2001; Sarma, 2004). The Arabian Sea is known for the second largest Tuna fishing region
64 in the Indian Ocean (Lee et al., 2005). The Somali and Omani upwelling regions experience
65 phytoplankton blooms that are prominent with Net Primary Production (NPP) exceeding 435 g C
66 m⁻² yr⁻¹ (Liao et al., 2016). On the other hand productivity over the SLD (Vinayachandran and
67 Yamagata, 1998) is triggered by open ocean Ekman suction with strong Chl-a blooms during the

68 summer monsoon (Murtugudde et al., 1999; Vinayachandran et al., 2004). Similarly, the SC
69 upwelling is basically due to the strong alongshore winds and its variation is associated with the
70 impact of equatorial and coastal Kelvin waves (Murtugudde et al., 2000, Valsala and Rao, 2016).
71 The interannual variability associated with the Java-Sumatra coastal upwelling is strongly
72 coupled with ENSO (El-Niño Southern Oscillation) through the Walker cell and Indonesian
73 throughflow (Susanto et al., 2001; Valsala et al., 2011) and peaks in July through August with a
74 potential new production of 0.1 Pg C yr^{-1} (Xing et al., 2012). The SCTR productivity has a large
75 spatial and interannual variability. The warmer upper ocean condition associated with El Niño
76 reduces the amplitude of subseasonal SST variability over the SCTR (Jung and Kirtman., 2016).
77 The Chl-a concentration peaks in summer when the southeast trade winds induce mixing and
78 initiate the upwelling of nutrient-rich water (Murtugudde et al., 1999; Wiggert et al., 2006;
79 Vialard et al., 2009; Dilmahamod et al., 2016).

80 Understanding the biological production and variability in the upwelling systems is important
81 because it gives us crucial information regarding marine ecosystem variability (Colwell, 1996;
82 Harvell et al., 1999). The observations also provide vital insights into physical and biological
83 interactions of the ecosystem (Naqvi et al., 2010) as well as the biophysical feedbacks
84 (Murtugudde et al., 2001), although limitations of sparse observations often force us to depend
85 on models to examine the large spatio-temporal variability of the ecosystem (Valsala et al.,
86 2013). Simple to intermediate complexity marine ecosystem models have been employed by
87 several of the previous studies (Sarmiento et al., 2000; Orr et al., 2001; Matsumoto et al., 2008).
88 However, the representation of marine ecosystem with proper parameterizations in models has
89 always been a daunting task. This is an impediment to the accurate representation of biological

90 primary and export productions in models (Friedrichs et al., 2006, 2007) and these issues also
91 impact the modeling of upper trophic levels (Lehodey et al., 2010).

92 Biological production can be quantified with a better understanding of primary production
93 which depends on water temperature, light and nutrient availability (Brock et al., 1993; Moisan
94 et al., 2002) and this became the key reason for parameterizing the production in models as one
95 or more combinations of these terms (Yamanaka et al., 2004). Any of these basic parameters can
96 be tweaked to alter production in models. For example, the availability of nutrients and light
97 determines the phytoplankton growth (Eppely et al., 1972) or growth rate (Boyd et al., 2013).
98 Stoichiometry and carbon-to-Chl-a ratios are other important factors to be considered in
99 modeling (Christian et al., 2001, Wang et al., 2009) but we will not consider them in this study.

100 The Ocean Carbon-cycle Model Intercomparison Project (OCMIP) greatly improved our
101 understanding of global carbon cycle (Najjar and Orr, 1998). OCMIP-II further introduced a
102 simple phosphate-dependent production term in biological models for long-term simulations of
103 the carbon cycle in response to anthropogenic climate change with an accurate annual mean state
104 (Najjar and Orr, 1998; Orr et al., 2001; Doney et al., 2004). However, the OCMIP – II model
105 simulations come with a penalty of strong seasonal biases when compared with observations
106 (Orr et al., 2003). In this protocol, the community compensation depth (hereinafter Z_c) is defined
107 as the depth at which photosynthesis equals entire community respiration and the irradiance at
108 which this balance achieved is the compensation irradiance (E_{com}). Note that Z_c is clearly
109 different from the conventional euphotic zone depth (Morel, 1988). Within Z_c , the production of
110 organic phosphorous representing the biological production (in the present context the Net
111 Community Production; NCP) is given as $J_{prod} = \frac{1}{\tau} ([PO_4] - [PO_4^*])$, where $[PO_4]$ is the model
112 phosphate concentration and $[PO_4^*]$ is observational phosphate concentration. τ is the restoration

113 timescale assumed to be 30 days. Whenever the model phosphate exceeds the observational
114 phosphate, it allows production. At Z_c , the NCP is zero and above Z_c the NPP exceeds the
115 community respiration and the ecosystem will grow (Smetacek and Passow, 1990; Gattuso et al.,
116 2006; Sarmiento and Gruber, 2006; Regaudix-de-Gioux and Duarte, 2010; Marra et al., 2014).
117 However, Z_c was held constant in time and space in OCMIP-II models (Najjar and Orr, 1998;
118 Matsumoto et al., 2008) because the OCMIP-II protocol takes the minimalistic approach to
119 biology and simplifies the model calculations with a very limited set of state variables suitable
120 for long term simulations when casted in coarse resolution models (Orr et al., 2005). Though in
121 reality Z_c varies in space and time (Najjar and Keeling, 1997) just as the euphotic zone depth
122 does as documented in ship measurements (Qasim, 1977, 1982). The variation in Z_c indicates
123 the seasonality of the production zone itself.

124 Most of the biophysical models prescribe a constant value for Z_c , e.g., a default value of
125 $Z_c = 75$ m in OCMIP –II protocol (Najjar and Orr, 1998) and $Z_c = 100$ m in Minnesota Earth
126 System Model (Matsumoto et al., 2008). Depending on the latitude, Z_c varies between 50m and
127 100m in the real world (Najjar and Keeling, 1997). In our study we have attempted a novel
128 biological parameterization scheme for spatially and temporally varying Z_c in the OCMIP–II
129 framework by representing the production as a function of solar radiation (Parsons et al., 1984)
130 and prescribed Chl-a. In this hypothesis, a spatially and temporally varying Z_c is estimated from
131 the vertical attenuation of insolation by the surface Chl-a. The depth at which the insolation
132 reaches the compensation irradiance (chosen as 10 Wm^{-2}) is taken as Z_c . Phosphorous is the
133 basic currency which limits the production within this varying Z_c . This spatially and temporally
134 varying Z_c represents the seasonality in the production zone which is lacking in the original
135 OCMIP-II protocol.

136 Regions of sustained upwelling like the eastern equatorial Pacific are well understood in
137 terms of the role of upwelling in increasing the surface water pCO₂ to drive an outgassing of CO₂
138 into the atmosphere (Feely et al., 2001; Valsala et al., 2014). The Indian Ocean on the other hand
139 experiences only seasonal upwelling which is relatively weak in the deep tropics but stronger off
140 the coasts of Somalia and Oman and in the SLD (Valsala et al., 2013). The relative importance of
141 the solubility vs. biological pump is not well understood. Our focus here on implementing
142 seasonality in Zc of OCMIP models nonetheless leads to new insights on the impact of improved
143 biological production on surface water pCO₂ and air-sea CO₂ fluxes. **The improvements due to
144 the effect of a variable Zc over the Indian Ocean and the sensitivity experiments where
145 upwelling is muted strongly imply that the biological pump may play as much of a role as the
146 solubility pump in determining surface pCO₂ and CO₂ fluxes over the Indian Ocean.**

147 The paper is organized as follows. Model, Data, and Methods are detailed in Section 2.
148 The spatially inhomogeneous Zc derived out of the new parameterization and its impact on
149 simulated seasonality of biology and carbon cycle are detailed in Section 3. Further ~~results and
150 discussion are followed in Section 4 and~~ a conclusion is given in Section 54.

151

152 **2. Model, Data, and Methods**

153 **2.1. Model**

154 The study utilizes the Offline Ocean Tracer Transport Model (OTTM; Valsala et al., 2008)
155 coupled with OCMIP biogeochemistry model (Najjar and Orr, 1998). OTTM does not compute
156 currents and stratifications (i.e., temperature and salinity) on its own. It is capable of accepting
157 any ocean model or data-assimilated product as physical drivers. The physical drivers prescribed

158 include 4-dimensional currents (u,v), temperature, salinity, and 3-dimensional mixed layer depth,
 159 surface freshwater and heat fluxes, surface wind stress and sea surface height. The resolution of
 160 the model setup is similar to the parent model from which it borrows the physical drivers. With
 161 the given input of Geophysical Fluid Dynamics Laboratory (GFDL) reanalysis data (Chang et.
 162 al., 2012), the zonal and meridional resolutions are 1° with 360 grid points longitudinally and 1°
 163 at higher latitudes but having a finer resolution of 0.8° in the tropics, with 200 latitudinal grid
 164 points. The model has 50 vertical levels with 10m increment in the upper 225m and stretched
 165 vertical levels below 225m. The horizontal grids are formulated in spherical coordinates and
 166 vertical grids are in z levels. The model employs a B-grid structure in which the velocities are
 167 resolved at corners of the tracer grids. The model uses a centered-in-space and centered-in-time
 168 (CSCT) numerical scheme along with an Asselin-Robert filter (Asselin, 1972) to control the
 169 ripples in CSCT.

170 The tracer concentration (C) evolves with time as

$$171 \quad \frac{\partial C}{\partial t} + U \cdot \nabla_H C + W \frac{\partial C}{\partial z} = \frac{\partial}{\partial z} K_z \frac{\partial C}{\partial z} + \nabla_H \cdot (K_h \nabla_H C) + J + F \quad (1)$$

172 where ∇_H is the horizontal gradient operator, U and W are the horizontal and vertical velocities
 173 respectively. K_z is the vertical mixing coefficient, and K_h is the two-dimensional diffusion
 174 tensor. J represents any sink or source due to the internal consumption or production of the
 175 tracer. F represents the emission or absorption of fluxes at the ocean surface. Here, the source
 176 and sink terms are provided through the biogeochemical model. Vertical mixing is resolved in
 177 the model using K- profile parameterization (KPP) (Large et al., 1994).

178 In addition to KPP, the model uses a background vertical diffusion reported by Bryan and Lewis
 179 (Bryan and Lewis, 1979). For horizontal mixing, model incorporates Redi fluxes (Redi, 1982)

180 and GM fluxes (Gent and McWilliams, 1990) which represent the eddy-induced variance in the
181 mean tracer transport. A weak Laplacian diffusion is also included in the model for
182 computational stability where the sharp gradient in concentration occurs.

183 2.2. Biogeochemical model

184 The biogeochemical model used in the study is based on the OCMIP – II protocol as
185 stated above. The main motivation of OCMIP–II protocol is to employ a minimalistic approach
186 to simulate the ocean carbon cycle with a nutrient restoration approach to calculate the oceanic
187 biological production (Najjar et al., 1992; Anderson and Sarmiento, 1995). The present version
188 of the model has four prognostic variables coupled with the circulation field, viz., inorganic
189 phosphate (PO_4^{3-}), dissolved organic phosphorus (DOP), dissolved inorganic carbon (DIC) and
190 alkalinity (ALK). The basic currency for the biological model is phosphorous because of the
191 availability of a more extensive phosphate database and to eliminate the complexities associated
192 with nitrogen fixation and denitrification. Detailed model equations and variables are introduced
193 in Appendix-A with brief description given below.

194 The production of organic phosphorus in the model using the nutrient restoring approach is given
195 by

$$196 \quad J_{prod} = \frac{1}{\tau}([PO_4] - [PO_4]^*) \quad (2)$$

$$197 \quad [PO_4] > [PO_4]^* ; Z < Z_c$$

$$198 \quad J_{prod} = 0 \quad (3)$$

$$199 \quad [PO_4] \leq [PO_4]^*$$

200 Where J_{prod} represents the biogeochemical flows with respect to production of organic
 201 phosphorous. $[PO_4]^*$ is the observed phosphate concentration and $\tau=30$ days is the restoration
 202 time scale (Najjar et. al., 1992).

203 The vertically integrated new production ($g\ C\ m^{-2}\ yr^{-1}$) in the model is defined as

$$New\ production = \int_{z_c}^0 -J_{prod}\ dz \quad (4)$$

204 The export production ($g\ C\ m^{-2}\ yr^{-1}$) in the model is calculated as given below

$$Export\ production = (1 - \sigma) \int_0^{z_c} J_{prod}\ dz \quad (5)$$

205 Air-sea CO_2 flux in the model is estimated by,

$$F = K_w \Delta pCO_2 \quad (6)$$

207 where K_w is gas transfer velocity and ΔpCO_2 is the difference in partial pressure of carbon
 208 dioxide between the ocean and atmosphere.

209 pCO_2 is calculated in the model by using DIC and ALK and is given by,

$$pCO_2 = \frac{[DIC]}{K_0} \frac{[H^+]^2}{[H^+]^2 + K_1[H^+] + K_1K_2} \quad (7)$$

210 Where $[H^+]$ is calculated using Newton-Raphson iterative method (Press et. al., 1996, Najjar and
 211 Orr, 1998). K_0 is the solubility constant of CO_2 and K_1 , K_2 are the dissociation constant for
 212 carbonic acid respectively (Sarmiento and Gruber, 2006, Weiss, 1974, Mehrbach et al., 1973,
 213 Dickson and Millero, 1987, Najjar and Orr, 1998).

214 Details of all parameters in the biogeochemical model and calculations of solubility and
215 biological pump are provided in Appendix-A. The design and validation of the physical model is
216 reported by Valsala et al., (2008, 2010) and biogeochemical model by Najjar and Orr (1998).

217

218 **2.3. Data**

219 For validating the model results, observational datasets of CO₂ flux and pCO₂ are taken
220 from Takahashi et al., (2009). Satellite-derived Net Primary Production (NPP) data were taken
221 from Sea-viewing Wide Field of view Sensor (SeaWiFS) Chl-a product, calculated using
222 Vertically Generalized Production Model (VGPM) (Behrenfeld and Falkowski, 1997). The NPP
223 data is scaled to export production (EP) by multiplying with an e-ratio (e = 0.37) representative
224 of Indian Ocean upwelling zones (Sarmiento and Gruber, 2006, Laws et al., 2000; Falkowski et
225 al., 2003). The initial conditions for PO₄ are taken from the World Ocean Atlas (Garcia et al.,
226 2014). Initial conditions for DIC and ALK are taken from the Global Ocean Data Analysis
227 Project (GLODAP; Key et al., 2004) dataset. The dissolved Organic Phosphorous (DOP) is
228 initialized with a constant value of 0.02 μmol kg⁻¹ (Najjar and Orr, 1998). The data sources and
229 citations are provided in the Acknowledgement.

230

231 **2.4. Methods**

232 A spin-up for 50 years from the given initial conditions is performed with the
233 climatological physical drivers. As the initial conditions are provided from a mean state of
234 observed climatology this duration of spin-up is sufficient to reach statistical equilibrium in the

235 upper 1000 m (Le Quere et al., 2000). Atmospheric pCO₂ has been set to a value from the 1950s
236 in the spin-up run for calculating the air-sea CO₂ exchange. A seasonal cycle of atmospheric
237 pCO₂ has been prescribed as in Keeling et al. (1995).

238 After the spin-up, an interannual simulation for 50 years from 1961 to 2010 has been
239 carried out with the corresponding observed atmospheric pCO₂ described in Keeling et al.,
240 (1995). The first five years of the interannual run were looped five times through the physical
241 fields of 1961 repeatedly for a smooth merging of the spin-up restart to the interannual physical
242 variables. Since the study is focused on bias corrections to the seasonal cycle of pCO₂ and DIC
243 with a variable Z_c, a model climatology for carbon cycle has been constructed from 1990 to
244 2010, which includes the anthropogenic increase of oceanic DIC in the climatological calculation
245 and is comparable with the Takahashi et al. (2009) observations.

246 Additional two sensitivity experiments have been performed separately by providing
247 annual mean currents or temperatures as drivers over selected regions of the basin in order to
248 segregate the role of varying Z_c in improving the seasonality of carbon cycle. The aim of these
249 sensitivity experiments is to understand how successful the new parameterization for Z_c is in
250 capturing the carbon cycle variability related to the upwelling episodes even though the seasonal
251 cycle in physics is suppressed. The model driven with annual mean currents **suppresses** the
252 effect of upwelling by muting the Ekman divergence over the region of interest. On the other
253 hand, the model forced with annual mean temperatures suppresses the cooling effect of
254 upwelling. A smoothing technique with linear interpolation ($u = u(1 - x) + \bar{u}x$) is applied to
255 the offline-data in order to blend the annual mean fields (\bar{u}) provided to the selected region with
256 the rest of the domain (u) in order to reduce a sudden transition at the boundaries. Here x
257 represents an index which varies between 0 and 1 within a distance of 10^0 from the boundaries of

258 the region of interest to the rest of the model domain. Results of sensitivity experiments are
259 provided in supplementary Material.

260

261 2.5. Community compensation depth (Z_c) parameterization

262 The OCMIP – II protocol separates the production and consumption zones by a depth termed
263 as compensation depth (Z_c); the depth at which photosynthesis is large enough to balance the
264 community respiration (i.e., both the autotrophic and heterotrophic respiration). At the
265 community compensation depth, the NCP is zero i.e., $NCP = NPP - R_h = 0$, (i.e., $NPP = GPP -$
266 R_a), GPP is gross primary production, and R_h and R_a are the heterotrophic and autotrophic
267 respirations, respectively (Smetacek and Passow, 1990; Najjar and Orr, 1998; Gattuso et al.,
268 2006; Regaudix-de-Gioux and Duarte, 2010; Marra et al., 2014). The light intensity at Z_c is
269 compensation irradiance (E_{com}), the irradiance at which the gross community primary production
270 balances respiratory carbon losses for the entire community (Gattuso et al., 2006; Regaudix-de-
271 Gioux and Duarte, 2010). We define a spatially and temporally varying compensation depth
272 (hereinafter $varZ_c$) as a depth where compensation irradiance (attenuated by surface Chl-a,
273 Jerlov et al., 1976) reaches a minimum value of 10 W m^{-2} . In this way, the $varZ_c$ has both spatio-
274 temporal variability of light as well as Chl-a. The Chl-a is given as monthly climatology as
275 constructed from satellite data. Observations show that the primary production reduces rapidly to
276 20% or less of the surface value below a threshold of 10 W m^{-2} (Parsons et al., 1984; Ryther,
277 1956; Sarmiento and Gruber, 2006). Moreover higher ocean temperatures (those in the tropics)
278 enhance the respiration rates resulting in high compensation irradiance (Parsons et al., 1984;
279 Ryther, 1956; Lopez-Urrutia et al., 2006; Regaudix-de-Gioux and Duarte, 2010). A study by

280 Regaudix-de-Gioux and Duarte (2010) reported the mean value of compensation irradiance over
281 the Arabian Sea as $0.4 \pm 0.2 \text{ mol photon m}^{-2} \text{ day}^{-1}$ which is close to $10 \text{ W m}^{-2} \text{ day}^{-1}$.

282 Figure 2 compares the scatter of average relative photosynthesis within varZc as a
283 function of solar radiation for the Indian Ocean (see Appendix-B). This encapsulates the
284 corresponding curve from the observations for the major phytoplankton species in the ocean such
285 as diatoms, green algae and dinoflagellates (Ryther et al., 1956; Parsons et al., 1984; Sarmiento
286 and Gruber, 2006). The model permits 100% production of organic phosphorus for radiation
287 above ~~50~~ 10 W m^{-2} . However the availability of phosphate concentration in the model acts as an
288 additional limit for production which indirectly represents the photoinhibition at higher
289 irradiance; for example, in the oligotrophic gyres.

290

291 3. Results and Discussions

292 The inclusion of seasonality in Zc by way of parameterizing varZc leads to a remarkable
293 spatio-temporal variability in Zc (Figure 3). Zc over the Arabian Sea varies from 10 m to 25 m
294 during December to February (DJF) and deepens down to 45 m during March to May (MAM)
295 due to the increase in the surface solar radiation. During the monsoon season i.e., June to
296 September (JJAS), Zc again shoals to 10 m - 35 m due to the attenuation of solar radiation by the
297 increased biological production (Chl-a). During October to November (OCT-NOV), Zc slightly
298 deepens as compared to JJAS.

299 The Bay of Bengal Zc deepens from 35 m to 40 m during DJF and further deepens to 50 m
300 during MAM when the solar radiation is maximum and biological production is minimum
301 (Prasannakumar et al., 2002). Further reduction of Zc can be seen through JJAS as a result of a

302 reduction in solar radiation during monsoon cloud cover. Z_c during OCT-NOV is 35 m on
303 average.

304 The equatorial Indian Ocean can be seen as a belt of 40 m - 45 m Z_c throughout the season
305 except for JJAS. During JJAS, a shallow Z_c is seen near the coastal Arabian Sea (around 10 m to
306 35 m) presumably due to the coastal Chl-a blooms. Deep Z_c off the coast of Sumatra (~ 40 m to
307 50 m) is found during JJAS. Java-Sumatra coastal upwelling is centered on September to
308 November (Susanto et al., 2001) and upwelling originates at around 100 m depth (Valsala and
309 Maksyutov, 2010; Xing et al., 2012).

310 Southward of 10°S in the oligotrophic gyre region, Z_c varies from 40 m to more than 60 m
311 throughout the year. A conspicuous feature observed while parameterizing the solar radiation
312 and Chl-a dependent Z_c is that its maximum value never crosses 75 m especially in the Indian
313 Ocean which is the value specified in OCMIP-II models. The cutoff depth of 75 m in OCMIP-II
314 is obtained from observing the seasonal variance in oxygen data (Najjar and Keeling, 1997) as an
315 indicator of the production zone. However, our results show that parameterizing a production
316 zone based on solar radiation and Chl-a predicts a production zone and its variability that is
317 largely less than 75 m. The relevance of $\text{var}Z_c$ in the seasonality of the modeled carbon cycle is
318 illustrated as follows.

319

320 **3.1. Simulated seasonal cycle of pCO_2 and CO_2 fluxes**

321 The annual mean biases in simulated CO_2 fluxes and pCO_2 were evaluated by comparing
322 with Takahashi et al., (2009) observations (Figure 4). The model biases are significantly reduced

323 with the implementation of varZc compared to that of the constant Zc (hereinafter constZc). A
324 notable reduction in pCO₂ bias (by ~ 10µatm) is observed along the WAS (Figure 4d).

325 In order to address the role of the new biological parameterization of a variable Zc, we
326 have extended our study by choosing four key regions where the biological production and CO₂
327 fluxes are prominent in the Indian Ocean with additional sensitivity experiments (see
328 Introduction and references therein). The regions (boxes shown in Figure 1) we considered are,
329 (1) Western Arabian Sea (WAS; 40°E:65°E, 5°S:25°N) (2) Sri Lanka Dome (SLD; 81°E:90°E,
330 0°:10°N) (3) Seychelles-Chagos Thermocline Ridge (SCTR; 50°E:80°E, 5°S:10°S) and (4)
331 Sumatra Coast (SC; 90°E:110°E, 0°:10°S; Figure 1). The seasonal variations of Zc over these
332 selected key regions are shown in Figure 5. A detailed analysis of CO₂ fluxes, pCO₂, biological
333 export and new productions and the impact of varZc simulations in improving the strength of
334 biological pump and solubility pump for these key regions are presented below.

335

336 **3.2. Western Arabian Sea (WAS)**

337 The WAS Zc has a double peak pattern over the annual cycle. During the February-March
338 period, Zc deepens down to a maximum of 43.85 ± 2.3 m into March and then shoals to $25.75 \pm$
339 1.5 m (Figure 5) during the monsoon period (uncertainty represents the interannual standard
340 deviations of monthly data from 1990-2010). This shoaling of Zc depth during the monsoon
341 indicates the potential ability of the present biological parameterization to capture the wind-
342 driven upwelling related production in the WAS. During the post-monsoon period, the second
343 deepening of Zc occurs during November with a maximum depth of 34.91 ± 2.2 m. The ability to
344 represent the seasonality of the production zone renders a unique improvement in CO₂ flux

345 variability especially in the WAS in comparison to the OCMIP-II experiments (Orr et al, 2003;
346 Figure 6a).

347 OCMIP –II simulations with a constZc of 75 m underestimate the CO₂ flux when compared
348 to the observations of Takahashi et al. (2009). This underestimation is clearly visible during the
349 monsoon period. Our simulations with the varZc resulted in a better seasonality of CO₂ flux
350 when compared with Takahashi et al. (2009) observations (Figure 6a). The improvement due to
351 the varZc scheme is able to represent the seasonality of CO₂ flux better especially during the
352 monsoon period when wind-driven upwelling is dominant. Obviously, the relative role of the
353 biological and solubility pumps have to be deciphered in this context.

354 The CO₂ flux during July from observations, constZc, and varZc simulations are 3.09 mol m⁻²
355 yr⁻¹, 1.82 ± 0.4 mol m⁻² yr⁻¹ and 3.10 ± 0.5 mol m⁻² yr⁻¹, respectively. Southwesterly wind-driven
356 upwelling over the WAS especially off the Somali coast (Smith and Codispoti, 1980; Schott,
357 1983; Smith, 1984) and Oman (Bruce, 1974; Smith and Bottero, 1977; Swallow, 1984; Bauer et
358 al., 1991), pulls nutrient-rich subsurface waters closer to the surface while the available turbulent
359 energy due to the strong winds lead to mixed layer entrainment of the nutrients resulting in a
360 strong surface phytoplankton bloom (Krey and Babenerd, 1976; Banse, 1987; Bauer, 1991;
361 Brock et al, 1991). This regional bloom extends over 700 km offshore from the Omani coast due
362 to upward Ekman pumping driven by strong, positive wind-stress curl to the northwest of the low
363 level jet axis and the offshore advection (Bauer et al., 1991; Brock et al., 1991; Brock and
364 McClain, 1992a, b; Murtugudde and Busalacchi, 1999, Valsala, 2009) resulting in strong
365 outgassing of CO₂ flux and an enhanced pCO₂ in the WAS (Valsala and Maksyutov, 2013;
366 Sarma et al., 2002). The seasonal mean CO₂ flux during the southwest monsoon period (JJAS)
367 for constZc and varZc simulations are 1.44 ± 0.2 mol m⁻² yr⁻¹ and 2.31 ± 0.4 mol m⁻² yr⁻¹,

368 respectively. The biological parameterization of varZc considerably improves the average CO₂
369 flux during the monsoon period by $0.86 \pm 0.1 \text{ mol m}^{-2} \text{ yr}^{-1}$. The annual mean CO₂ flux from
370 observations, constZc and varZc simulations are $0.94 \text{ mol m}^{-2} \text{ yr}^{-1}$, $0.80 \pm 0.17 \text{ mol m}^{-2} \text{ yr}^{-1}$ and
371 $1.07 \pm 0.2 \text{ mol m}^{-2} \text{ yr}^{-1}$, respectively. The annual mean CO₂ flux is improved by $0.27 \pm 0.05 \text{ mol}$
372 $\text{m}^{-2} \text{ yr}^{-1}$.

373 Seasonality in pCO₂ also shows a remarkable improvement during the southwest monsoon
374 period (Figure 6b). The pCO₂ with constZc is considerably lower at a value of $385.22 \pm 3.5 \text{ } \mu\text{atm}$
375 during June compared to observational values of $392.83 \text{ } \mu\text{atm}$. However, varZc simulation
376 performs better in terms of pCO₂ variability. The peak value of pCO₂ reaches up to 405.42 ± 5.8
377 μatm . The seasonal mean pCO₂ during the Southwest monsoon period from observations,
378 constZc, and varZc simulations are $397.58 \text{ } \mu\text{atm}$, $389.18 \pm 3.6 \text{ } \mu\text{atm}$ and $399.95 \pm 5.0 \text{ } \mu\text{atm}$,
379 respectively. The improvement in pCO₂ by varZc simulation is $10.76 \pm 1.3 \text{ } \mu\text{atm}$ when compared
380 with the constZc simulation. This inherently infers that constZc simulation fails to capture the
381 pCO₂ driven by upwelling during the Southwest monsoon while the varZc simulation is
382 demonstrably better in representing this seasonal increase. The annual mean pCO₂ from
383 observations, constZc, and varZc simulations are $394.69 \text{ } \mu\text{atm}$, $389.62 \pm 3.9 \text{ } \mu\text{atm}$ and $391.19 \pm$
384 $4.7 \text{ } \mu\text{atm}$, respectively. However, it is worth mentioning that there are parts of the year where the
385 constZc performs better compared to varZc. For instance, during MAM as well as in November,
386 the constZc simulation yielded a better comparison with the observed pCO₂ whereas varZc
387 simulation yields a reduced magnitude of pCO₂. This may well indicate the biological vs.
388 solubility pump controls on pCO₂ during the intermonsoons. The role of mesoscale variability in
389 the ocean dynamics may also play a role (Valsala and Murtugudde, 2015). Nevertheless, during

390 the most important season (JJAS) when the pCO₂, CO₂ fluxes, and biological production are
391 found to be dominant in the Arabian Sea, the varZc produces a better simulation.

392 The improvements shown by the use of varZc in the simulation of CO₂ flux and pCO₂ can be
393 elicited by further analysis of the model biological production. Figure 7 shows the comparison of
394 model export production and new production with observational export production from
395 satellite-derived NPP for constZc and varZc simulations. The model export production in the
396 constZc simulation is much weaker when compared to varZc simulation. The varZc simulation
397 has improved the model export production. Theoretically, the new and export productions in the
398 model should be in balance with each other (Eppley and Peterson, 1979). The constZc export
399 production is much weaker than new production and it is not in balance. In contrast, the varZc
400 simulation yields a close balance among them.

401 Compared with the observational export production which peaks in August at a value of
402 154.78 g C m⁻² yr⁻¹, the varZc simulated export and new productions peak at a value of 160.44 ±
403 20.4 g C m⁻² yr⁻¹ and 167.18 ± 24.0 g C m⁻² yr⁻¹, respectively, but in July. A similar peak can be
404 observed in constZc simulated new production as well, with a value of 178.19 ± 28.0 g C m⁻² yr⁻¹.
405 This apparent shift of one month during JJAS in the model export production as well as in the
406 new production is noted as a caveat in the present set up which will need further investigation.
407 Arabian Sea production is not just limited by nutrients but also the dust inputs (Wiggert et al.,
408 2006). The dust-induced primary production in the WAS, especially over the Oman coast is
409 noted during August (Liao et al., 2016). The mesoscale variability in the circulation and its
410 impact on production and carbon cycle are also a limiting factor in this model as noted above.

411 The seasonal mean export production during the southwest monsoon period from satellite-
412 derived estimate is $123.57 \text{ g C m}^{-2} \text{ yr}^{-1}$, whereas for constZc and varZc simulations it is $84.81 \pm$
413 $16.0 \text{ g C m}^{-2} \text{ yr}^{-1}$ and $147.19 \pm 23.8 \text{ g C m}^{-2} \text{ yr}^{-1}$, respectively. The new biological
414 parameterization strengthens the model export production by $62.38 \pm 7.8 \text{ g C m}^{-2} \text{ yr}^{-1}$ for the
415 southwest monsoon period, which is over a 70% increase. This indicates a considerable impact
416 of the biological pump in the model simulated CO_2 flux and pCO_2 over the WAS. For constZc
417 simulation, the computed new production is slightly higher ($150.84 \pm 27.9 \text{ g C m}^{-2} \text{ yr}^{-1}$) than that
418 of varZc ($133.03 \pm 19.5 \text{ g C m}^{-2} \text{ yr}^{-1}$). The annual mean export production from observations,
419 constZc and varZc simulations are $94.31 \text{ g C m}^{-2} \text{ yr}^{-1}$, $77.41 \pm 15.1 \text{ g C m}^{-2} \text{ yr}^{-1}$ and 122.54 ± 25.2
420 $\text{g C m}^{-2} \text{ yr}^{-1}$, respectively.

421 To understand how the varZc parameterization strengthens the export production in the
422 model, we have analyzed the phosphate profiles. It appears that the varZc parameterization
423 allows more phosphate concentration (Figure 8a, b) in the production zone and thereby increases
424 the corresponding biological production (Figure 8c, d). The net export production in the model
425 during JJAS is consistent with the satellite data (Figure 7b). However, in the constZc case, the
426 exports are rather 'flat' throughout the season with the imperfect representation of seasonal
427 biological export. The Table 1-4 summarize all the values discussed here.

428 The impact of varZc in the biological and solubility pumps is computed as per Louanchi et
429 al., (1996, see Appendix A). The varZc parameterization has strengthened the biological as well
430 as the solubility pump in the model and thereby modifying the phosphate profiles and achieves a
431 seasonal balance in export versus new production (Figure 9a). During the monsoon period, the
432 varZc simulation increases the strength of the solubility and biological pumps by $10.43 \pm 1.3 \text{ g C}$
433 $\text{m}^{-2} \text{ yr}^{-1}$ and $106.52 \pm 9 \text{ g C m}^{-2} \text{ yr}^{-1}$, respectively (see Table 5 and 6). Similarly, the annual mean

434 strength of solubility pump and the biological pump is increased by $3.29 \pm 0.6 \text{ g C m}^{-2} \text{ yr}^{-1}$ and
435 $81.18 \pm 9.92 \text{ g C m}^{-2} \text{ yr}^{-1}$, respectively. This supports the fact that the varZc parameterization
436 basically modifies the biological and solubility pumps in the model simulation and thereby
437 improves the seasonal cycle of CO_2 flux and pCO_2 .

438

439 **3.3 Sri Lanka Dome (SLD)**

440 The seasonal variation in Zc for SLD has a similar pattern as that of WAS. Zc deepens to its
441 maximum during March up to $45.23 \pm 0.3 \text{ m}$ and reaches its minimum during the following
442 monsoon period at $30.79 \pm 1.5 \text{ m}$ (Figure 5). The similarities of varZc between WAS and SLD
443 indicates that they both are under similar cycles of solar influx and biological production. The
444 SLD Chl-a dominates only up to July (Vinayachandran et al., 2004) which explains why
445 production with varZc increases earlier compared to WAS which occurs during August-October.

446 The seasonality in CO_2 flux and pCO_2 were compared with Takahashi et al., (2009)
447 observations (Figure 10). varZc results in a slight improvement in CO_2 flux when compared with
448 constZc (Figure 10a). However, both constZc and varZc simulations underestimate the
449 magnitude of CO_2 flux when compared with observations. The seasonal mean CO_2 flux during
450 the monsoon period is $1.79 \text{ mol m}^{-2} \text{ yr}^{-1}$ from observations, which means SLD region is a source
451 of CO_2 . But the mean values of constZc and varZc simulations yield flux values of -0.008 ± 0.2
452 $\text{mol m}^{-2} \text{ yr}^{-1}$ and $0.24 \pm 0.2 \text{ mol m}^{-2} \text{ yr}^{-1}$, respectively. The constZc simulation misrepresents the
453 SLD region as a sink of CO_2 during monsoon period which is opposite to that of observations.
454 The varZc simulation corrects this misrepresentation to a source albeit at a smaller magnitude by

455 $0.24 \pm 0.09 \text{ mol m}^{-2} \text{ yr}^{-1}$ for the monsoon period. Compared to observations, the varZc case
456 underestimates the magnitude of JJAS mean by $1.55 \text{ mol m}^{-2} \text{ yr}^{-1}$.

457 The annual mean CO₂ fluxes for constZc and varZc simulations are $-0.02 \pm 0.1 \text{ mol m}^{-2} \text{ yr}^{-1}$
458 and $0.10 \pm 0.2 \text{ mol m}^{-2} \text{ yr}^{-1}$, respectively. The varZc parameterization leads to an improvement of
459 $0.13 \pm 0.1 \text{ mol m}^{-2} \text{ yr}^{-1}$ in the annual mean CO₂ flux when compared with constZc simulation.
460 The observational annual mean of CO₂ flux is $0.80 \text{ mol m}^{-2} \text{ yr}^{-1}$ which is highly underestimated
461 by both simulations. This indicates a regulation of biological production of the region by varZc
462 which makes this region a source of CO₂ during monsoon. The role of the solubility pump may
463 also be underestimated due to the biases in the physical drivers and the lack of mesoscale eddy
464 activities in these simulations (Prasanna Kumar et al., 2002; Valsala and Murtugudde, 2015).

465 The seasonality of pCO₂ (Figure 10b) especially in the monsoon period is significantly
466 improved. The mean pCO₂ during the monsoon season from observation over the SLD region is
467 $382.44 \text{ } \mu\text{atm}$. The seasonal mean pCO₂ during monsoon period for constZc and varZc
468 simulations are $371.67 \pm 6.04 \text{ } \mu\text{atm}$ and $379.24 \pm 8.9 \text{ } \mu\text{atm}$, respectively. The annual mean pCO₂
469 from observations, constZc, and varZc simulations are $380.21 \text{ } \mu\text{atm}$, $370.76 \pm 6.1 \text{ } \mu\text{atm}$ and
470 $374.94 \pm 9.6 \text{ } \mu\text{atm}$, respectively. varZc simulations improve the JJAS mean pCO₂ by 7.56 ± 2.8
471 μatm and the annual mean pCO₂ by $4.18 \pm 3.5 \text{ } \mu\text{atm}$, which is reflected in CO₂ flux as well. This
472 is likely due to the impact of new biological parameterization in capturing the episodic upwelling
473 in the SLD region which is further investigated by looking at its biological production.

474 The SLD biological production is highly exaggerated by the model for both constZc and
475 varZc simulations (Figure 11a, b). The seasonal mean biological export for the monsoon period
476 is $51.54 \text{ g C m}^{-2} \text{ yr}^{-1}$ as per satellite-derived estimates. However, the constZc and varZc

477 simulations overestimate it at $167.71 \pm 59.04 \text{ g C m}^{-2} \text{ yr}^{-1}$ and $151.51 \pm 46.4 \text{ g C m}^{-2} \text{ yr}^{-1}$,
478 respectively. This exaggerated export is visible in climatological annual means where for
479 constZc and varZc simulations they are $144.43 \pm 49.8 \text{ g C m}^{-2} \text{ yr}^{-1}$ and $156.08 \pm 43.8 \text{ g C m}^{-2} \text{ yr}^{-1}$,
480 respectively.

481 For constZc simulation, new production is overestimated from March to October when
482 compared to observations and the second peak is observed in November (Figure 11a). But the
483 overestimate in new production with varZc is observed only during JJAS period by a value of
484 $26.23 \text{ g C m}^{-2} \text{ yr}^{-1}$. For the SLD region, the varZc parameterization overestimates the export
485 production but minimizes the excess new production, especially in the monsoon period by 64.15
486 $\pm 36.4 \text{ g C m}^{-2} \text{ yr}^{-1}$. This indicates that the varZc parameterization is somewhat successful in
487 capturing the upwelling episode during the monsoon over SLD. All values are summarized in
488 Table 1 to 4.

489 The solubility and biological pumps are modified by the varZc parameterization significantly
490 when compared with the constZc simulation (Figure 9b). Over the monsoon period, the strength
491 of the solubility and biological pumps are improved by $2.81 \pm 1.1 \text{ g C m}^{-2} \text{ yr}^{-1}$ and $66.68 \pm 9.7 \text{ g}$
492 $\text{C m}^{-2} \text{ yr}^{-1}$, respectively. Similarly, the annual mean strength of solubility and biological pump
493 are increased by $0.99 \pm 1.2 \text{ g C m}^{-2} \text{ yr}^{-1}$ and $52.5 \pm 5.1 \text{ g C m}^{-2} \text{ yr}^{-1}$ respectively. All values are
494 provided in Table 5 and 6.

495

496 **3.4 Sumatra Coast (SC)**

497 The seasonal variation in Zc over the SC region lies between 40 m and 46 m (Figure 5). The
498 seasonal maximum occurs during January to March, especially in March with a depth of 45.5 m.

499 During the monsoon period, Z_c shoals slightly with a minimum of 41.1 m in July. The variation
500 in Z_c is relatively small as compared to the other regions which is consistent with its relatively
501 low production throughout the year.

502 The seasonality of CO_2 flux and pCO_2 captured by constZc and varZc simulations are shown
503 in Figure 12a, b. The varZc simulations overestimate both CO_2 flux and pCO_2 , especially during
504 the monsoon. It is found that the constZc simulation is better compared to varZc simulation. The
505 varZc simulation overestimates the seasonal mean CO_2 flux and pCO_2 by $1.19 \text{ mol m}^{-2} \text{ yr}^{-1}$ and
506 $29.61 \text{ } \mu\text{atm}$, respectively, compared to observations (Table 1). However, constZc produces a
507 better estimate compared with observations for CO_2 flux and pCO_2 . The constZc simulation
508 delivers a better annual mean than varZc (Table 1, 2). The annual mean bias in constZc and
509 varZc simulations for CO_2 flux is $-0.0033 \text{ mol m}^{-2} \text{ yr}^{-1}$ and $0.31 \text{ mol m}^{-2} \text{ yr}^{-1}$, respectively.
510 Similarly, pCO_2 bias is $1.95 \text{ } \mu\text{atm}$ and $9.07 \text{ } \mu\text{atm}$ for constZc and varZc simulations.

511 Biological production simulated by the model along SC explains the overestimation of CO_2
512 flux and pCO_2 (Figure 13). Both constZc and varZc simulations greatly overestimate export
513 production in the model. However, a small enhancement in the new production during JJAS in
514 constZc case is an indicator of upwelling episodes. The seasonal mean new production during
515 the monsoon from constZc and varZc are $63.64 \pm 30.9 \text{ g C m}^{-2} \text{ yr}^{-1}$ and $78.11 \pm 29.1 \text{ g C m}^{-2} \text{ yr}^{-1}$,
516 respectively (Table 4). The seasonal mean export production during the monsoon from
517 observations is $58.87 \text{ g C m}^{-2} \text{ yr}^{-1}$ (Table 3). The constZc simulation represents a better new
518 production, which is seen as a relatively small exaggeration of CO_2 flux and pCO_2 . The
519 biological response of SC is found to be better with constZc which is in contradiction to a
520 general improvement found with varZc in the other regions examined here. Such discrepancies
521 over the SC could be due to the effect of Indonesian Throughflow (Bates et al., 2006) which is

522 not completely resolved in the model due to coarse spatial resolution (also see Valsala et al.,
523 2010).

524 The overestimation of export production by varZc simulation is also evident by the increase
525 in strength of the biological and solubility pumps, respectively (Figure 9c). The annual mean and
526 JJAS mean DIC increases in the production zone due to the biological pump is $67.21 \pm 1.3 \text{ g C}$
527 $\text{m}^{-2} \text{ yr}^{-1}$ and $83.62 \pm 0.5 \text{ g C m}^{-2} \text{ yr}^{-1}$, respectively. Similarly the increase in DIC due to the effect
528 of solubility pump during the JJAS period and annual mean are $10.95 \pm 5.2 \text{ g C m}^{-2} \text{ yr}^{-1}$ and 3.87
529 $\pm 2.2 \text{ g C m}^{-2} \text{ yr}^{-1}$ respectively (see table 5 and 6).

530

531 **3.5 Seychelles-Chagos Thermocline Ridge (SCTR)**

532 The SCTR is a unique open-ocean upwelling region with a prominent variability in air-sea
533 interactions (Xie et al., 2002). Wind-driven mixing and upwelling of subsurface nutrient-rich
534 water play a major role in the biological production of this region (Dilmahamod et al., 2016).
535 The seasonal cycle in Zc is shown in Figure 5. The maximum Zc occurs in November at about
536 44.94 m and the minimum at 33.2 m in July. The shoaling of Zc during the monsoon period
537 shows that the biological parameterization captures the upwelling response over this region.

538 The seasonality of CO₂ flux and pCO₂ are shown in Figure 14. The Takahashi observations
539 of CO₂ flux shows a peak in June with outgassing of CO₂ during the upwelling episodes.
540 However, both constZc and varZc simulations underestimate this variability. The seasonality of
541 CO₂ flux in varZc shows a significant improvement when compared to constZc simulation, but
542 underestimated when compared to observations. The seasonal mean CO₂ flux during the
543 monsoon from observations, constZc and varZc simulations are $0.82 \text{ mol m}^{-2} \text{ yr}^{-1}$, -0.32 ± 0.3

544 $\text{mol m}^{-2} \text{yr}^{-1}$ and $-0.05 \pm 0.4 \text{ mol m}^{-2} \text{yr}^{-1}$, respectively. This represents a reduction in the seasonal
545 mean sink of CO_2 flux in the SCTR region during the monsoon by $0.27 \pm 0.1 \text{ mol m}^{-2} \text{yr}^{-1}$
546 bringing it closer to a source region (see Table 1 for details).

547 The improved CO_2 flux is also supported by the seasonal cycle in pCO_2 . Based on
548 observations, the seasonal mean of pCO_2 with constZc during JJAS is underestimated by 11.47
549 μatm , varZc simulation underestimates it by $6.45 \mu\text{atm}$. So it is evident that varZc simulation
550 capture the upwelling episodes better, marked by a larger pCO_2 during JJAS period. However,
551 the magnitude of pCO_2 is still underestimated compared to observations (Table 2).

552 Figure 15 shows the biological production of constZc and varZc simulations for SCTR. It is
553 clear that both simulations overestimate the export production and underestimate the new
554 production. The JJAS mean export production from observations, constZc and varZc are 51.08 g
555 $\text{C m}^{-2} \text{yr}^{-1}$, $57.39 \pm 14.2 \text{ g C m}^{-2} \text{yr}^{-1}$ and $99.23 \pm 29.8 \text{ g C m}^{-2} \text{yr}^{-1}$, respectively. The varZc
556 simulations exaggerate the model export production by $48.14 \text{ g C m}^{-2} \text{yr}^{-1}$. The varZc simulation
557 improves the JJAS mean new production by $1.14 \pm 2.2 \text{ g C m}^{-2} \text{yr}^{-1}$ (Table 4). The DIC variations
558 due to the biological pump over the monsoon period and the annual mean also support the
559 exaggerated export production. During the monsoon period, the varZc simulation strengthens the
560 biological and solubility pump by $72.64 \pm 6.2 \text{ g C m}^{-2} \text{yr}^{-1}$ and $-4.56 \pm 1.6 \text{ g C m}^{-2} \text{yr}^{-1}$,
561 respectively when compared to the constZc simulation (Figure 9d). This is also reflected in the
562 annual mean DIC variations due to the biological and solubility pump effects (see table 5 and 6).
563 This slight improvement in the model new production, especially during the monsoon period
564 signals that the varZc better captures the upwelling over SCTR. Considering the annual mean
565 values of model export and new production, constZc simulation is reasonably faithful to
566 observations.

567 The underestimation of CO₂ and pCO₂, as well as the exaggeration of model export
568 production and a slight, overestimate in model new production may be due to two reasons; (1)
569 SCTR is a strongly coupled region with remote forcing of the mixed layer – thermocline
570 interactions (Zhou et al., 2008) which can affect the seasonality in biological production that the
571 model may not be resolving reasonably, (2) the bias associated with physical drivers, especially
572 wind stress may underestimate the CO₂ flux as well biological production. A similar
573 overestimation of biological production was also reported in a coupled biophysical model
574 (Dilmahamod et al., 2016).

575 Table 1 – 4 shows the entire summary of seasonal and annual mean CO₂ flux, pCO₂ and
576 biological production reported in Section 3.

577

578 **4. Sensitivity Simulations**

579 ~~From the analysis of four major upwelling regions over the Indian Ocean, it is evident that~~
580 ~~the biological parameterization of varZc better captures upwelling episodes and thus it enhances~~
581 ~~the model export production. This is most clearly visible over the WAS region. In order to~~
582 ~~quantify how much the varZc parameterization contributes to the seasonality of carbon cycle,~~
583 ~~two additional sensitivity simulations are carried out; viz. (1) with annual mean offline currents~~
584 ~~and (2) annual mean offline temperatures with the goal of suppressing the dynamical and~~
585 ~~thermodynamical effects of seasonal upwelling over WAS (see Section 2 for details). The focus~~
586 ~~on this region is motivated by its prominence as the most productive zone of the Indian Ocean.~~
587 ~~Moreover, the improvement in the biological processes in the model by the varZc~~
588 ~~parameterization is best captured in this region. The results are discussed below.~~

589

590 **~~4.1 Impact of varZc parameterization on seasonality of carbon cycle with annual~~**
591 **~~mean currents.~~**

592 ~~To quantify the impact of varZc parameterization, the model is forced with annual mean~~
593 ~~currents only over WAS region with unaltered currents in the rest of the ocean. The hypothesis is~~
594 ~~that the muting of the seasonal variability of Ekman divergence removes the upwelling and the~~
595 ~~biological pump contribution to production and carbon cycle. The comparison of constZc and~~
596 ~~varZc then allows us to decipher the impact of varZc in capturing the impacts of upwelling on~~
597 ~~biological production and the carbon cycle. The smooth blending of currents at the boundary of~~
598 ~~the WAS domain is achieved by a linear smoothing function as given in Section 2.~~

599 ~~The model biological responses (inferred by comparing with the control run) in terms of the~~
600 ~~CO₂ flux shows a flat pattern over the monsoon period for constZc simulation (see~~
601 ~~supplementary material; Figure 16 S1(a)). While the varZc simulation forced with the annual~~
602 ~~mean currents shows an enhanced CO₂ flux indicating the outgassing of CO₂ flux over WAS due~~
603 ~~to wind-driven upwelling (Figure 16b S1(b)). This qualitatively shows that the varZc itself has~~
604 ~~improved the seasonality in the biological processes (export and new production) and captured~~
605 ~~the upwelling episodes during the monsoon. The varZc parameterization is responsible for an~~
606 ~~improvement of $0.48 \pm 0.04 \text{ mol m}^{-2} \text{ yr}^{-1}$ and $0.13 \pm 0.02 \text{ mol m}^{-2} \text{ yr}^{-1}$ in the JJAS seasonal and~~
607 ~~annual mean CO₂ fluxes, respectively. This improves the overall model CO₂ flux in the control~~
608 ~~run especially in July (Figure 16b S1(b)).~~

609 ~~—— Similar improvements are also noticed in pCO₂ (Figure 17 S2). In the constZc simulation~~
610 ~~with annual mean currents, the pCO₂ dips down during JJAS monsoon period which indicates~~

611 ~~the inadequacy of constZc in capturing the upwelling enriched pCO₂ difference (Figure 17 S2(a,~~
612 ~~b)). The varZc simulation slightly modifies the pCO₂ in the ‘right’ direction during JJAS despite~~
613 ~~the annual mean currents.~~

614 ~~———— The export and new productions in the model explain the modification of CO₂ flux and~~
615 ~~pCO₂ by varZc parameterization. The biological export production is highly underestimated in~~
616 ~~the constZc simulation forced with annual mean currents while the varZc simulation captures the~~
617 ~~seasonal upswing in production (Figure 18 S3). The improved JJAS mean and annual mean~~
618 ~~export production by $43.51 \pm 8.6 \text{ g C m}^{-2} \text{ yr}^{-1}$ and $30.28 \pm 13.7 \text{ g C m}^{-2} \text{ yr}^{-1}$, respectively is a clear~~
619 ~~indication of the positive impacts of a varZc. Similarly, the improvement in JJAS mean and~~
620 ~~annual mean new production (Figure 19 S4) from varZc simulated with annual mean currents are~~
621 ~~$17.39 \pm 0.8 \text{ g C m}^{-2} \text{ yr}^{-1}$ and $14.81 \pm 0.1 \text{ g C m}^{-2} \text{ yr}^{-1}$, respectively. In short the varZc biological~~
622 ~~parameterization improves the export and new productions in the model. This helps the model to~~
623 ~~capture the upwelling episodes over the study regions. Table 7 S1 summarizes all the results of~~
624 ~~biological sensitivity runs.~~

625 ~~————~~

626 ~~4.2 Impact of varZc parameterization on seasonality of carbon cycle with annual~~ 627 ~~mean temperatures.~~

628 ~~By imposing the annual mean temperature over WAS region, we are suppressing the cooling~~
629 ~~effect of temperature due to upwelling and quantifying how much the model seasonality is~~
630 ~~improved due to varZc parameterization. (see Section 2 for details). The varZc simulations~~
631 ~~forced with annual mean SST has larger JJAS mean and annual mean CO₂ fluxes by 0.88 ± 0.1~~
632 ~~$\text{mol m}^{-2} \text{ yr}^{-1}$ and $0.28 \pm 0.07 \text{ mol m}^{-2} \text{ yr}^{-1}$, respectively (Figure 20 S5 and Table 8 S2). For a given~~

633 ~~annual mean SST the solubility pump largely controls the CO₂ emission during JJAS if a varZc~~
634 ~~is prescribed, likely by the enrichment of DIC (inferred from Figure 8b). Similarly, the~~
635 ~~improvement in pCO₂ (Figure 21 S6) with varZc simulation is also remarkable. The JJAS mean~~
636 ~~and annual mean improvements from the implementation of varZc are $11.05 \pm 1.9 \mu\text{atm}$ and 1.91~~
637 ~~$\pm 1.4 \mu\text{atm}$, respectively. The detailed quantification of CO₂ and pCO₂ responses for this~~
638 ~~experimental setup is given in Table 8 S2. The above analysis adds supporting evidence that the~~
639 ~~varZc simulation strengthens the seasonality of the model compared to the constZc case. This is~~
640 ~~presumably accomplished by the more accurate Zc and production zone implied with a variable~~
641 ~~Zc.~~

642

643 **4. Summary and Conclusions**

644 A spatially and temporally varying Zc parameterization as a function of solar radiation and
645 Chl-a is implemented in the biological pump model of OCMIP-II for a detailed analysis of
646 biological fluxes in the upwelling zones of the Indian Ocean. The varZc parameterization
647 improves the seasonality of model CO₂ flux and pCO₂ variability, especially during the monsoon
648 period. A significant improvement is observed in WAS where the monsoon wind-driven
649 upwelling dominates biological production. The magnitude of CO₂ flux matches with
650 observations, especially in July when monsoon winds are at their peak. Monsoon triggers
651 upwelling in SLD as well which acts as a source of CO₂ to the atmosphere. The seasonal and
652 annual mean are underestimated with constZc and the SLD is reduced to a sink of CO₂ flux. The
653 varZc simulation modifies the seasonal and annual means of the CO₂ flux of SLD and depict it as
654 a source of CO₂ especially during the monsoon, but the magnitude is still underestimated

655 compared to Takahashi et al. (2009) observations. The SCTR variability is underestimated by
656 both constZc and varZc simulations, portraying it as a CO₂ sink region whereas observations
657 over the monsoon period indicate that the thermocline ridge driven by the open ocean wind-
658 stress curl is, in fact, an oceanic source of CO₂. However, the varZc simulation reduces the
659 magnitude of the sink in this region bringing it relatively close to observations.

660 VarZc biological parameterization strengthens the export and new productions in the model,
661 which allows it to represent a better seasonal cycle of CO₂ flux and pCO₂ over the study regions.
662 The WAS export production is remarkably improved by $62.37 \pm 7.8 \text{ g C m}^{-2} \text{ yr}^{-1}$ compared to
663 constZc. This supports our conclusion that the varZc parameterization increases the strength of
664 biological export in the model. Over the SLD, the JJAS seasonal mean export and new
665 production are underestimated in varZc compared to constZc simulations, but the annual mean
666 export production is improved. Export production at SC and SCTR are highly exaggerated and
667 there is hardly any improvement in new production with a variable Zc especially over the
668 monsoon period. The inability of varZc parameterization to improve the seasonality of SC and
669 SCTR may be due to the interannual variability of biological production associated with the
670 Indonesian throughflow and remote forcing of the mixed layer-thermocline interactions and the
671 effect of biases in the wind stress data used as a physical driver in the model.

672 Sensitivity experiments carried out by prescribing annual mean currents or temperatures over
673 selected subdomains reveal that the varZc retains the seasonality of carbon fluxes, pCO₂, and
674 export and new productions closer to observations. This strongly supports our contention that
675 varZc parameterization improves export and new productions and it is also efficient in capturing
676 upwelling episodes of the study regions. This points out the significant role of having a close
677 balance in seasonal biological export and new production in models to capture the seasonality in

678 the carbon cycle. This also confirms the role of biological and solubility pumps in producing the
679 seasonality of carbon cycle in the upwelling zones.

680 However, the underestimation of the seasonality of CO₂ flux over the SLD and
681 overestimation over the SC as well as the SCTR are a cautionary flag for the study. This
682 uncertainty poses an important scientific question as to whether the model biology over the SC
683 and SCTR region is not resolving the seasonality in CO₂ flux and pCO₂ properly or whether the
684 seasonality in the Z_c is not able to fully capture the biological processes.

685 To address these questions we have used an inverse modeling approach (Bayesian inversion)
686 in order to optimize the spatially and temporally varying Z_c using surface pCO₂ as the
687 observational constraint and computed the optimized biological production. The results will be
688 reported elsewhere.

689

690

691

692

693

694

695

696

697 **Appendix – A**

698 The time evolution equations of the model variables are given by

$$\frac{d[PO_4]}{dt} = L([PO_4]) + J_{PO_4} \quad (A1)$$

$$\frac{d[DOP]}{dt} = L([DOP]) + J_{DOP} \quad (A2)$$

$$\frac{dDIC}{dt} = L([DIC]) + J_{DIC} + J_g DIC + J_v DIC \quad (A3)$$

$$\frac{d[ALK]}{dt} = L([ALK]) + J_{ALK} + J_v ALK \quad (A4)$$

699 Where L is the 3D transport operator, which represents the effects of advection, diffusion, and
 700 convection. [] or square brackets indicate the concentrations in mol m⁻³. $J_{PO_4}, J_{DOP}, J_{DIC}, J_{ALK}$ **is**
 701 **are** the biological source/sink terms and $J_v DIC, J_v ALK$ are the virtual source-sink terms
 702 representing the changes in surface DIC and ALK, respectively, due to evaporation and
 703 precipitation. $J_g DIC$ is the source-sink term due to air-sea exchange of CO₂.

704 The following equations represent for the biological processes in the model

705 For $Z < Z_c$,

$$706 \quad J_{prod} = \frac{1}{\tau}([PO_4] - [PO_4^*]), \quad [PO_4] > [PO_4^*] \quad (A5)$$

$$707 \quad J_{DOP} = \sigma J_{prod} - \kappa[DOP] \quad (A6)$$

$$708 \quad J_{PO_4} = -J_{prod} + \kappa[DOP] \quad (A7)$$

$$709 \quad J_{ca} = Rr_{C:P}(1 - \sigma)J_{prod} \quad (A8)$$

$$710 \quad J_{DIC} = r_{C:P}J_{PO4} + J_{ca} \quad (A9)$$

$$711 \quad J_{ALK} = -r_{N:P}J_{PO4} + 2J_{ca} \quad (A10)$$

712 For $Z > Z_c$,

$$713 \quad J_{prod} = 0, \quad [PO_4] \leq [PO_4^*] \quad (A11)$$

$$714 \quad J_{DOP} = -\kappa[DOP] \quad (A12)$$

$$715 \quad J_{PO4} = -\frac{\partial F}{\partial Z} + \kappa[DOP] \quad (A13)$$

$$716 \quad F_c = (1 - \sigma) \int_0^{Z_c} J_{prod} dZ \quad (A14)$$

$$717 \quad F(Z) = F_c \left(\frac{Z}{Z_c}\right)^a \quad (A15)$$

$$718 \quad J_{ca} = -\frac{\partial F_{ca}}{\partial Z} \quad (A16)$$

$$719 \quad F_{ca} = Rr_{C:P}F_c e^{-(Z-Z_c)/d} \quad (A17)$$

720 Where Z is the depth and Z_c is the compensation depth in the model. ~~J_{DOP} and J_{PO4} are the~~
721 ~~biogeochemical sources and sinks and~~ J_{prod} , J_{ca} represents the biogeochemical flows with
722 respect to production and calcification. Within Z_c , the production of organic phosphorous in the
723 model J_{prod} is calculated using equation A5. $[PO_4]$ is the model phosphate concentration and
724 $[PO_4^*]$ is observational phosphate. τ is the restoration timescale assumed to be 30 days. Whenever
725 the model phosphate exceeds the observational phosphate, it allows production, below which the
726 production is zero. The observational phosphate data were taken from the World Ocean Atlas

727 (WOA; Garcia et al., 2014). It is assumed that a fixed fraction (σJ_{prod}) of phosphate uptake is
 728 converted into Dissolved Organic Phosphorus (DOP) which is a source for J_{DOP} (equation A6).
 729 The phosphate not converted to DOP results in an instantaneous downward flux of particulate
 730 organic phosphorus at Z_c (equation A14). The decrease of flux with depth due to
 731 remineralization is shown by a power law relationship as in equation A15. The values of the
 732 constants a , κ , σ are 0.9, 0.2/year to 0.7/year, 0.67, respectively. The rate of production is used to
 733 explain the formation of calcium carbonate cycle in surface waters (equation A8) and its export
 734 is given by equation A16, where R is the rain ratio, a constant molar ratio of exported particulate
 735 organic carbon to the exported calcium carbonate flux at Z_c . The exponential decrease of
 736 calcium carbonate flux with scale depth d is given by equation A17. The biological source or
 737 sink of dissolved inorganic carbon (DIC) and alkalinity (ALK) is explained through equations
 738 A9 and A10, respectively. Where the values of rain ratio (R) is taken as 0.07 and the Redfield
 739 ratio, $r_{C:P} = 117$, and $r_{N:P} = 16$ and scale depth d is chosen as 3500m.

740

741 **Biological and Solubility Pump calculations**

742 The biological effect on DIC is calculated from Louanchi et al., (1996). The tendency of DIC
 743 due to biomass production and calcite formation in the production zone is expressed as below.

$$744 \quad \left(\frac{\partial DIC}{\partial t}\right)_b = \left(\frac{\partial PO_4}{\partial t}\right)_b \times R_{C:P} - J_{Ca} \quad (A18)$$

745 The total tendency of DIC in the production zone is:

$$746 \quad \left(\frac{\partial DIC}{\partial t}\right)_{total} = \left(\frac{\partial DIC}{\partial t}\right)_b + \int_x \int_y F dx dy \quad (A19)$$

747 where $\left(\frac{\partial DIC}{\partial t}\right)_b$ is the evolution of DIC due to the impact of biology (i.e., biological pump). The
748 first term in the R.H.S of Equation A18 is the rate of change of phosphate resulting from
749 photosynthesis and respiration in the model (i.e., J_{po4} in this case) multiplied by the carbon to
750 phosphorous Redfield ratio ($R_{C:P} = 117:1$) and J_{Ca} represents the calcite formation in the model
751 (see Equation A8 & A16). The solubility pump is calculated as the surface integral of the flux F
752 (Louanchi et al., 1996).

753

754 **Appendix B**

755 In order to compare our model production of organic phosphorous to the curve of Ryther et al.,
756 (1956) we have merely scaled our total production to “relative photosynthesis”, which is,
757 according to Ryther et al., (1956) **is** an index between 0 and 1 indicating the strength of
758 production estimated as P_1/P_{max} . Here P_1 is the photosynthesis at each intensity (of light) of
759 different species and P_{max} is the maximum photosynthesis observed in the same control
760 experiment. The curve between relative photosynthesis and light intensity shows the relation
761 between photosynthetic activity and light in marine phytoplankton. Since our method relates
762 biological production to a function of light (limitation) by Chl-a attenuation, it is the best curve
763 to cross-compare our results. In this case we scaled our total biological production within Z_c into
764 relative values between 0-1 by P_1/P_{max} . in which P_1 is taken as the individual grid cell biological
765 component of organic phosphorus production and P_{max} is the maximum production available in
766 the domain at any given instant. All the grid points are quite similar to the curve of Ryther et al.,
767 (1956) as shown in Figure 2.

768

769 **Acknowledgements**

770 Thanks to two anonymous reviewers and the editor (Marilaure Grégoire) for comments. Sreeush
771 M. G. sincerely acknowledges the fellowship support from Indian Institute of Tropical
772 Meteorology (IITM) to carry out the study. The OCMIP-II routines were taken from
773 (<http://ocmip5.ipsl.jussieu.fr/OCMIP/>). GFDL data for OTTM is taken from
774 (<http://data1.gfdl.noaa.gov/nomads/forms/assimilation.html>). Takahashi data is taken from
775 (<http://www.ldeo.columbia.edu/res/pi/CO2/>) and SeaWiFS data is obtained from the National
776 Aeronautics and Space Administration (NASA) Ocean Color Website
777 (<http://oceancolor.gsfc.nasa.gov/>). The computations were carried out in High-Performance
778 Computing (HPC) facility of Ministry of Earth Sciences (MoES), IITM.

779

780

781

782

783

784

785

786

787

788 **References**

789 Anderson, L. A., Sarmiento, J. L.: Global ocean phosphate and oxygen simulations, *Global*
790 *Biogeochem. Cycles*, 9, 621-636, doi:10.1029/95GB01902, 1995.

791 Asselin, R.: Frequency filter for time integrations, *Mon. Wea. Rev.*, 100, 487–490, doi:
792 [10.1175/1520-0493.1972](https://doi.org/10.1175/1520-0493.1972).

793 Banse, K., McClain, C. R.: Winter blooms of phytoplankton in the Arabian Sea as observed by
794 the Coastal Zone Color Scanner, *Mar. Ecol. Prog. Ser.*, 34, 201 – 211, 1986.

795 Banse, K.: Seasonality of phytoplankton chlorophyll in the central and northern Arabian Sea,
796 *Deep Sea Res.*, 34, 713 – 723, doi:10.1016/0198-0149, 1987.

797 Barber, R. T., Marra, J., Bidigare, R. C., Codispoti, L. A., Halpern, D., Johnson, Z., Latasa, M.,
798 Goericke, R., and Smith, S. L.: Primary productivity and its regulation in the Arabian Sea during
799 1995, *Deep. Sea. Res. pt. II*, 48, 1127 – 1172. doi:10.1016/S0967-0645, 2001.

800 Bates, N. R., Pequignet, A. C., and Sabine, C. L.: Ocean carbon cycling in the Indian Ocean: 2.
801 Estimates of net community production, *Global Biogeochem. Cycles.*, 20, GB3021,
802 doi:10.1029/2005GB002492, 2006.

803 Bauer, S., Hitchcock, G. L., Olson, D. B.: Influence of monsoonally-forced Ekman dynamics
804 upon surface-layer depth and plankton biomass distribution in the Arabian Sea, *Deep Sea Res.*,
805 38, 531 – 553, doi:10.1016/0198-0149, 1991.

806 Behrenfeld, M. J., Falkowski, P. G.: Photosynthetic rates derived from satellite-based
807 chlorophyll concentration, *Limnol. Oceanogr.*, 42, 1 – 20, doi: 10.4319/lo.1997.42.1.0001, 1997.

808 Boyd, P. W., Rynearson, T. A., Armstrong, E. A., Fu, F., Hayashi, K. and co-authors.: Marine
809 Phytoplankton Temperature versus growth responses from polar to tropical waters – outcome of
810 a scientific community-wide study, PLoS ONE 8(5), e63091,
811 Doi:10.1371/journal.pone.0063091, 2013.

812 Brock, J. C., McClain, C. R.: Interannual variability of the southwest monsoon phytoplankton
813 bloom in the north-western Arabian Sea, J. Geophys. Res., 97(C1), 733 – 750,
814 doi/10.1029/91JC02225, 1992.

815 Brock, J. C., McClain, C. R., Hay, W. W.: A southwest monsoon hydrographic climatology for
816 the northwestern Arabian Sea, J. geophys. Res., 97(C6), 9455 – 9465, doi: 10.1029/92JC00813,
817 1992.

818 Brock, J. C., McClain, C. R., Luther, M. E., Hay, W. W.: The phytoplankton bloom in the
819 northwestern Arabian Sea during the southwest monsoon of 1979, J. Geophys. Res., 96(C11),
820 623 – 642, doi: 10.1029/91JC01711, 1991.

821 Brock, J., Sathyendranath, S., and Platt, T.: Modelling the seasonality of subsurface light and
822 primary production in the Arabian Sea, Mar. Eco. Prog. Ser., 101, 209 – 221, 1993.

823 Bruce, J. G.: Some details of upwelling off the Somali and Arabian coasts, J. Mar. Res., 32, 419
824 – 423, 1974.

825 Bryan, K., Lewis, L. J.: A water mass model of the world ocean, J. Geophys. Res., 84, 2503 –
826 2517, doi: 10.1029/JC084iC05p02503, 1979.

827 Chang, Y. S., Zhang. S., Rosati. A., Delworth. T., Stern. W. F.: An assessment of oceanic
828 variability for 1960-2010 from the GFDL ensemble coupled data assimilation, *Clim. Dyn.*, 40,
829 775 – 803, doi: 10.1007/s00382-012-1412-2, 2012.

830 Christian J. R., Verschall M. A., Murtugudde R., Busalacchi A. J., McClain C. R.:
831 Biogeochemical modeling of the tropical Pacific Ocean. II: Iron biogeochemistry, *Deep Sea*
832 *Res.*, 49, 545 – 565, doi:10.1016/S0967-0645, 2001.

833 Colwell, R. R.: Global climate and infectious disease: the cholera paradigm, *Science.*, 274(5295),
834 2025 – 2031, doi: 10.1126/science.274.5295.2025, 1996.

835 Dickson, A. G., and F. J. Millero.: A comparison of the equilibrium constants for the dissociation
836 of carbonic acid in seawater media, *Deep-Sea Res.*, 34, 1733 – 1743, 1987.

837 Dilmahamod A. F., Hermes. J. C., Reason C. J. C.: Chlorophyll-a variability in the Seychelles-
838 Chagos Thermocline Ridge: Analysis of a coupled biophysical model, *J. of. Mar. Sys.*, 154, 220
839 – 232, doi:10.1016/j.jmarsys.2015.10.011, 2016.

840 Doney S. C., and co-authors.: Evaluating global ocean carbon models: The importance of
841 realistic physics, *Glob. Biogeochem. Cycles*, 18, doi:10.1029/2003GB002150, 2004.

842 Eppley, R. W., Peterson. B. J.: Particulate organic matter flux and planktonic new production in
843 the deep ocean, *Nature*, 282, 677-680, doi:10.1038/282677a0, 1979.

844 Eppley, R. W.: Temperature and phytoplankton growth in the sea, *Fish. Bull.*, 70, 1063 – 1085,
845 1972.

846 Falkowski, P. G., E. A. Laws, R. T. Barber, and J. W. Murray: phytoplankton and their role in
847 the primary, new and export production, In: Fasham M.J.R (eds) *Ocean Biogeochemistry*, Global

848 Change – The IGBP series (closed). Springer, Berlin, Heidelberg, doi:
849 https://doi.org/10.1007/978-3-642-55844-3_5, 2003.

850 Feely, R. A., Sabine, C. L., Takahashi, T., Wanninkhof, R.: Uptake and Storage of Carbon
851 Dioxide in the Ocean: The Global CO₂ Survey, *Oceanography.*, 14(4), 18–32,
852 doi:[10.5670/oceanog.2001.03](https://doi.org/10.5670/oceanog.2001.03), 2001.

853 Friedrichs, M. A. M., and co-authors.: Assessment of skill and portability in regional
854 biogeochemical models: role of multiple planktonic groups, *J. Geophys. Res.*, 112, doi:
855 [10.1029/2006JC003852](https://doi.org/10.1029/2006JC003852), 2007.

856 Friedrichs, M. A. M., Hood, R. R., Wiggert, J. D.: Ecosystem complexity versus physical forcing
857 quantification of their relative impact with assimilated Arabian Sea data, *Deep Sea Res.*, 53, 576-
858 600, doi:[10.1016/j.dsr2.2006.01.026](https://doi.org/10.1016/j.dsr2.2006.01.026), 2006.

859 Garcia, H. E., R. A. Locarnini, T. P. Boyer, J. I. Antonov, O.K. Baranova, M.M. Zweng, J.R.
860 Reagan, D.R. Johnson.: *World Ocean Atlas 2013, Volume 4: Dissolved Inorganic Nutrients*
861 (phosphate, nitrate, silicate), S. Levitus, Ed., A. Mishonov Technical Ed.; NOAA Atlas NESDIS
862 76, 25 pp, 2014.

863 Gattuso, J. P., B. Gentili, C. M. Duarte, J. A. Kleypas, J. J. Middelburg, and D. Antoine.: Light
864 availability in the coastal ocean: Impact on the distribution of benthic photosynthetic organisms
865 and their contribution to primary production, *Biogeosciences*, 3, 489 – 513, doi:[10.5194/bg-3-](https://doi.org/10.5194/bg-3-489-2006)
866 [489-2006](https://doi.org/10.5194/bg-3-489-2006), 2006.

867 Gent, P. R., McWilliams. J. C.: Isopycnal mixing in ocean circulation models, *J. Phys.*
868 *Oceanogr.*, 20, 150 – 155, doi: [10.1175/15200485](https://doi.org/10.1175/15200485), 1990.

869 Harwell, C., Kim, K., Burkholder, J., Colwell, R., Epstein, P. R., Grimes, D., Hofmann, E. E.,
870 Lipp, E. K., Osterhaus, A., and Overshreet, R. M.: Emerging marine diseases-climate links and
871 anthropogenic factors, *Science.*, 285(5433), 1505 – 1510, doi: 10.1126/science.285.5433.1505,
872 1999.

873 Howden, S., Murtugudde, R.: Effects of river inputs into the Bay of Bengal, *J. Geophys. Res.*,
874 106, 19,825-19,843. doi: 10.1029/2000JC000656, 2001.

875 Jerlov N. G.: *Marine optics*, Second ed., Elsevier, pp 231, 1976.

876 Jung, E., and Kirtman. B. P.: ENSO modulation of tropical Indian ocean subseasonal variability,
877 *Geophys. Res. Lett.*, 43, doi: 10.1002/2016GL071899, 2016.

878 Keeling, C. D., Whorf, T. P., Wahlen, M., and van der plicht, J.: Interannual extremes in the rate
879 of rise of atmospheric carbon dioxide since 1980, *Nature*, 375, 666 – 670, 1995.

880 Key, R. M., et al.,: A global ocean carbon climatology: Results from Global Data Analysis
881 Project (GLODAP), *Global Biogeochem. Cycles*, 18, GB4031, doi:10.1029/2004GB002247,
882 2004

883 Krey, J., Bahenerd, B.: *Phytoplankton production atlas of the international Indian Ocean*
884 *expedition*, Institut fur Meereskundeander Universitat Kiel, Kiel, German, 1976.

885 Laws, E. A., P. G. Falkowski, W.O. Smith, Jr., H. Ducklow and J. J. McCarthy: Temperature
886 effects on export production in the open ocean, *Global Biogeochem. Cycles*, 14, 1231 – 1246.

887

888 Large, W. G., McWilliams, J. C., Doney, S. C.: Oceanic vertical mixing: A review and a model
889 with a nonlocal boundary layer parameterization, *Rev. Geophys.*, 32, 363 – 403, doi:
890 10.1029/94RG01872, 1994.

891 Le Quere, C., Orr, J. C., Monfray, P., Aumont, O.: Interannual variability of the oceanic sink of
892 CO₂ from 1979 through 1997, *Global Biogeochem. Cycles.*, 14, p1247 – 1265, doi:
893 10.1029/1999GB900049, 2000.

894 Lee, P. F., Chen, I. C., Tzeng, W. N.: Spatial and Temporal distributions patterns of bigeye tuna
895 (*Thunnus obsesus*) in the Indian Ocean, *Zoological studies-Taipei*-, 44(2), 260, 2005.

896 Lehodey .P., Senina I., Sibert. J., Bopp. L., Calmettes B., Hampton .J., Murtugudde. R.:
897 Preliminary forecasts of Pacific bigeye tuna population trends under the A2 IPCC scenario, *Prog*
898 *in Oceanography.*, 86, 302 – 315, [doi:10.1016/j.pocean.2010.04.021](https://doi.org/10.1016/j.pocean.2010.04.021), 2010.

899 Liao, X., Zhan, H., Du, Y.: Potential new production in two upwelling regions of the Western
900 Arabian Sea: Estimation and comparison, *J. Geophys. Res. Oceans.*, 121,
901 [doi:10.1002/2016JC011707](https://doi.org/10.1002/2016JC011707), 2016.

902 Lopez-Urrutia, A., E. San Martin, R. P. Harris, and X. Irigoien.: Scaling the metabolic balance of
903 the oceans, *Proc. Natl. Acad. Sci. U.S.A.*, 103, 8739-8744, [doi:10.1073/pnas.0601137103](https://doi.org/10.1073/pnas.0601137103), 2006.

904 Louanchi. F., N. Metzl., and Alain Poisson.: Modelling the monthly sea surface f_{CO2} fields in the
905 Indian Ocean, *Marine Chemistry*, 55, 265 – 279, 1996.

906 Marra, J. F., Veronica P. Lance, Robert D. Vaillancourt, Bruce R. Hargreaves.: Resolving the
907 ocean's euphotic zone, *Deep Sea. Res. pt. I.*, 83, 45 -50, [doi:10.1016/j.dsr.2013.09.005](https://doi.org/10.1016/j.dsr.2013.09.005), 2014.

908 Matsumoto K., Tokos. K. S., Price., A. R., Cox. S. J.: First description of the Minnesota Earth
909 System Model for Ocean biogeochemistry (MESMO 1.0), *Geosci. Model Dev.*, 1, 1-15,
910 doi:10.5194/gmd-1-1-2008, 2008.

911 McCreary, J., Murtugude, R., Vialard, J., Vinayachandran, P., Wiggert, J. D., Hood, R. R.,
912 Shankar, D., Shetye, S.: Biophysical processes in the Indian Ocean, *Indian Ocean*
913 *Biogeochemical Processes and Ecological Variability.*, 9 – 32, doi: 10.1029/GM185, 2009.

914 Mehrbach, C., C. H. Culberson, J. E. Hawley, and R. M. Pytkowicz.: Measurement of the
915 apparent dissociation constants of carbonic acid in seawater at atmospheric pressure, *Limnol.*
916 *Oceanogr.*, 18, 897 – 907, 1973.

917 Moisan, J. R., Moisan, A. T., Abbott, M. R.: Modelling the effect of temperature on the
918 maximum growth rates of phytoplankton populations, *Eco. Modelling.*, 153, 197-215,
919 [doi:10.1016/S0304-3800\(02\)00008](https://doi.org/10.1016/S0304-3800(02)00008), 2002.

920 Morel, A.: Optical modeling of the upper ocean in relation to its biogenous matter content (Case
921 1 Waters), *J. Geophys. Res.*, 93, 10479-10, 768, doi: 10.1029/JC093iC09p10749, 1988.

922 Murtugudde R., McCreary J. P., Busalacchi, A. J.: Oceanic processes associated with anomalous
923 events in the Indian Ocean with relevance to 1997-1998, *J. Geophys. Res.*, 105, 3295-3306, doi:
924 10.1029/1999JC900294, 2000.

925 Murtugudde, R., Busalacchi, A. J.: Interannual variability of the dynamics and thermodynamics
926 of the tropical Indian Ocean, *J. Clim.* 12, 2300-2326, doi:10.1175/1520-0442, 1999.

927 Murtugudde, R., Seager, R., Thoppil, P.: Arabian Sea response to monsoon variations,
928 *Paleoceanography.*, 22, PA4217, doi:10.1029/2007PA001467, 2007.

929 Najjar, R. G., Keeling, R. F.: Analysis of the mean annual cycle of the dissolved oxygen
930 anomaly in the world ocean, *J. Mar. Res.*, 55, 117 – 151, doi:10.1357/0022240973224481, 1997.

931 Najjar, R. G., Orr, J. C.: Design of OCMIP-2 simulations of chlorofluorocarbons, the solubility
932 pump and common biogeochemistry, <http://www.ipsl.jussieu.fr/OCMIP/>, 1998.

933 Najjar, R. G., Sarmiento, J. L., Toggweiler, J. R.: Downward transport and fate of organic matter
934 in the ocean: simulations with a general circulation model, *Global Biogeochem. Cycles.*, 6, 45-
935 76, doi/10.1029/91GB02718, 1992.

936 Naqvi, S. W. A., Moffett, J. W., Gauns, M. U., Narvekar, P. V., Pratihary, A. K., Naik, H.,
937 Shenoy, D. M., Jayakumar, D. A., Goepfert, T. J., Patra, P. K., Al-Azri, A., and Ahmed, S. I.:
938 The Arabian Sea as a high-nutrient, low-chlorophyll region during the late Southwest Monsoon,
939 *Biogeosciences.*, 7, 2091-2100, doi:10.5194/bg-7-2091-2010, 2010.

940 Naqvi, S., Naik, H., Narvekar, P.: The Arabian Sea, in *Biogeochemistry*, edited by K. Black and
941 G. Shimmield, pp. 156 – 206, Blackwell, Oxford, 2003.

942 Orr, J. C., and co-authors.: Anthropogenic ocean acidification over the twenty-first century and
943 its impact on calcifying organisms, *Nature*, 437, 681 – 686, doi:10.1038/nature04095, 2005.

944 Orr, J. C., and co-authors.: Estimates of anthropogenic carbon uptake from four three-
945 dimensional global ocean models, *Glob. Biogeochem. Cycles.*, 15, p43 – 60, doi:
946 10.1029/2000GB001273, 2001.

947 Orr, J. C., Aumont, O., Bopp, L., Calderia, K., Taylor, K., et. al.: Evaluation of seasonal air-sea
948 CO₂ fluxes in the global carbon cycle models, International open Science conference (Paris, 7-
949 10 Jan. 2003), 2003.

950 Osawa, T., Julimantoro, S.: Study of fishery ground around Indonesia archipelago using remote
951 sensing data, International archives of the Photogrammetry, Remote sensing and spatial
952 information science., vol XXXVIII, part-8, 2010.

953 Parsons, T. R., Takahashi, M., Habgrave, B.: In Biological Oceanographic Processes, 3rd ed.,
954 330pp., Pergamon Press, New York, doi: 10.1002/iroh.19890740411, 1984.

955 Prasanna Kumar, .S., Muraleedharan, P. M., Prasad, T. G., Gauns, M., Ramaiah, N., de Souza, S.
956 N., Sardesai, S., Madhupratap, M.: Why is the Bay of Bengal less productive during summer
957 monsoon compared to the Arabian Sea?, Geophys. Res. Lett., 29(24), 2235,
958 doi:10.1029/2002GL016013, 2002.

959 Prasanna Kumar, S., Roshin, P. R., Narvekar, J., Dinesh Kumar, P., Vivekanandan, E.: What
960 drives the increased phytoplankton biomass in the Arabian Sea?, Current Science, 99(I), 101 –
961 106, 2010.

962 Prassana Kumar. S, Ramaiah. N, Gauns. M., Sarma V. V. S. S., Muraleedharan. P. M.,
963 RaghuKumar. S., Dileep Kumar., Madhupratap. M.: Physical forcing of biological productivity
964 in the Northern Arabian Sea during the Northeast Monsoon, Deep Sea Res. Pt. II., 48, 1115-
965 1126, [doi:10.1016/S0967-0645\(00\)00133-8](https://doi.org/10.1016/S0967-0645(00)00133-8), 2001.

966 Praveen, V., Ajayamohan, R. S., **Valsala**, V., Sandeep, S.: Intensification of upwelling along
967 Oman coast in a warming scenario, Geophys. Res. Lett., 43, doi:10.1002/2016GL069638, 2016.

968 Qasim, S. Z.: Biological productivity of the Indian Ocean, J. Mar. Sci., 6, 122 – 137, 1977.

969 Qasim, S. Z.: Oceanography of Northern Arabian Sea, Deep Sea Res., 29(9A), 1041 – 1068,
970 [doi:10.1016/0198-0149\(82\)90027-9](https://doi.org/10.1016/0198-0149(82)90027-9), 1982.

971 Redi, M.: Oceanic isopycnal mixing by coordinate rotation, *J. Phys. Oceanogr.*, 12, 1154 – 1158,
972 doi: [10.1175/1520-0485.1982](https://doi.org/10.1175/1520-0485.1982).

973 Regaudie-de-Gioux, A., and C. M. Duarte.: Compensation irradiance for planktonic community
974 metabolism in the ocean, *Global Biogeochem. Cycles*, 24, GB4013,
975 doi:10.1029/2009GB003639, 2010.

976 Roxy, M. K., Modi, A., Murtugudde, R., Valsala, V., Panickal, S., Prasanna Kumar, S.,
977 Ravichandran, M., Vichi, M., Levy, M.: A reduction in marine primary productivity driven by
978 rapid warming over the tropical Indian Ocean, 43, 826 – 833, *J. Geophys. Res. Letters.*,
979 doi:10.1002/2015GL066979, 2015.

980 Ryther, J., Menzel, D.: On the production, composition, and distribution of organic matter in the
981 Western Arabian Sea, *Deep Sea Research and Oceanographic Abstracts.*, 12(2), 199 -209.
982 doi:10.1016/0011-7471(65)90025-2, 1965.

983 Ryther, J.: Photosynthesis in the ocean as function of light Intensity, *Limnol. Oceanogr.*, vol 1,
984 issue 1, doi: 10.4319/lo.1956.1.1.0061, 1956.

985 Sarma V. V. S. S.: Net plankton community production in the Arabian Sea based on O₂ mass
986 balance model, *Glob. Biogeochem. Cycles.*, 18, GB4001, doi:10.1029/2003GB002198, 2004.

987 Sarma, V. V. S. S.: An evaluation of physical and biogeochemical processes regulating the
988 perennial suboxic conditions in the water column of the Arabian Sea, *Global Biogeochem.*
989 *Cycles.*, 16, doi:10.1029/2001GB001461, 2002.

990 Sarmiento, J. L., and Gruber, N.: *Ocean Biogeochemical Dynamics*, Princeton University Press,
991 New Jersey, 2006.

992 Sarmiento, J. L., Monfray. P., Maier-Reimer., Aumont, O., Murnane, R. J., Orr, J. C.: Sea-air
993 CO₂ fluxes and carbon transport: A comparison of three ocean general circulation models,
994 *Global Biogeochem. Cycles.*, 14, p1267 – 1281. doi: 10.1029/1999GB900062, 2000.

995 Schott, F.: Monsoon response of the Somali current and associated upwelling, *Prog.Oceanogr.*,
996 12, 357 – 381, [doi:10.1016/0079-6611\(83\)90014-9](https://doi.org/10.1016/0079-6611(83)90014-9), 1983.

997 Smetacek, V., and Passow, U.: Spring bloom initiation and Sverdrup's critical depth model,
998 *Limnol. Oceanogr.*, 35, 228 – 234, doi: 10.4319/lo.1990.35.1.0228, 1990.

999 Smith, L. S.: Understanding the Arabian Sea: Reflections on the 1994-1996 Arabian Sea
1000 Expedition, *Deep Sea Res. Pt. II.*, 48, 1385-1402, [doi:10.1016/S0967-0645\(00\)00144-2](https://doi.org/10.1016/S0967-0645(00)00144-2), 2001.

1001 Smith, R. L., Bottero, L. S.: On upwelling in the Arabian Sea. In Angel, M (ed) *A voyage of*
1002 *Discovery*. Pergamon Press, New York, p. 291 – 304, 1977.

1003 Smith, S. L., Codispoti, L. A.: Southwest monsoon of 1979: chemical and biological response of
1004 Somali coastal waters. *Science*, 209, 597 – 600. doi:[10.1126/science.209.4456.597](https://doi.org/10.1126/science.209.4456.597), 1980.

1005 Smith, S. L.: Biological indications of active upwelling in the northwestern Indian Ocean in 1964
1006 and 1979, a comparison with Peru and northwest Africa, *Deep Sea Res.*, 31, 951 – 967,
1007 [doi:10.1016/0198-0149\(84\)90050-5](https://doi.org/10.1016/0198-0149(84)90050-5), 1984.

1008 Susanto. R., Gordon, A. L., Zheng. Q.: Upwelling along the coasts of Java and Sumatra and its
1009 relation to ENSO, *J. Geophys. Res. Lett.*, 28, 1599-1602, doi: 10.1029/2000GL011844, 2001.

1010 Swallow, J. C.: Some aspects of the physical oceanography of the Indian Ocean, *Deep Sea Res.*,
1011 31, 639 – 650, [doi:10.1016/0198-0149\(84\)90032-3](https://doi.org/10.1016/0198-0149(84)90032-3), 1984.

1012 Takahashi, T., Sutherland, S. C., Wanninkhof, R., Sweeney, C., Feely, R. A., Chipman, D. W.,
1013 Hales, B., Friederich, G., Chavez, F., Sabine, C., et al.: Climatological mean and decadal
1014 changes in surface ocean pCO₂ and net sea-air CO₂ flux over the global oceans. Deep Sea Res.,
1015 Pt. II., 56, 554 – 557, [doi:10.1016/j.dsr2.2008.12.009](https://doi.org/10.1016/j.dsr2.2008.12.009), 2009.

1016 Valsala V., R. R. Rao.: Coastal Kelvin waves and dynamics of gulf of Aden eddies, Deep Sea
1017 Res., Pt. I., 116, 174 – 186, <https://doi.org/10.1016/j.dsr.2016.08.003>, 2016.

1018 Valsala V., Maksyutov, S.: A short surface pathway of the subsurface Indonesian Throughflow
1019 water from the Java Coast associated with upwelling, Ekman Transport, and Subduction. Int. J.
1020 Oceanogr., 15, doi: 10.1155/2010/540743, 2010.

1021 Valsala V., Maksyutov, S.: Interannual variability of air-sea CO₂ flux in the north Indian Ocean,
1022 Ocean Dynamics., 1 – 14, doi 10.1007/s10236-012-0588-7, 2013.

1023 Valsala, K. V., Maksyutov, S., Ikeda, M.: Design and Validation of an offline oceanic tracer
1024 transport model for a carbon cycle study, J. clim., 21, doi: 10.1175/2007JCLI2018.1, 2008.

1025 **Valsala, V.**, Maksyutov, S., Murtugudde, R.: Interannual to Interdecadal Variabilities of the
1026 Indonesian Throughflow Source Water Pathways in the Pacific Ocean, J. Phys. Oceanogr., 41,
1027 1921–1940, doi: [10.1175/2011JPO4561.1](https://doi.org/10.1175/2011JPO4561.1), 2011.

1028 Valsala, V., Maksyutov, S.: Simulation and assimilation of global ocean pCO₂ and air-sea CO₂
1029 fluxes using ship observations of surface ocean pCO₂ in a simplified biogeochemical model,
1030 Tellus., 62B, doi: 10.1111/j.1600-0889.2010.00495, 2010.

1031 **Valsala, V.**, Murtugudde, R.: Mesoscale and Intraseasonal Air-Sea CO₂ Exchanges in the
1032 Western Arabian Sea during Boreal Summer, Deep Sea Res. Pt. I, 103, 103-113,
1033 doi:[10.1016/j.dsr.2015.06.001](https://doi.org/10.1016/j.dsr.2015.06.001), 2015.

1034 **Valsala, V.**, Roxy, M., Ashok, K., Murtugudde, R.: Spatio-temporal characteristics of seasonal
1035 to multidecadal variability of pCO₂ and air-sea CO₂ fluxes in the equatorial Pacific Ocean, J.
1036 Geophys. Res., 119, 8987 – 9012, doi:[10.1002/2014JC010212](https://doi.org/10.1002/2014JC010212), 2014.

1037 Valsala, V.: Different spreading of Somali and Arabian coastal upwelled waters in the northern
1038 Indian Ocean: A case study. J. Phy. Oceanogr., 803 – 816, doi: [https://doi.org/10.1007/s10872-](https://doi.org/10.1007/s10872-009-0067-z)
1039 [009-0067-z](https://doi.org/10.1007/s10872-009-0067-z), 2009.

1040 Vialard, J. and co-authors.: Air-Sea Interactions in the Seychelles-Chagos Thermocline Ridge
1041 Region, BAMS, doi:[10.1175/2008BAMS2499.1](https://doi.org/10.1175/2008BAMS2499.1), 2009.

1042 Vinayachandran P. N., Shankar D., S. Vernekar, K. K. Sandeep, P. Amol, C. P. Neema and A.
1043 Chatterjee.: A summer monsoon pump to keep the bay of Bengal salty, Geophys. Res. Lett., 40,
1044 1777 – 1782, doi:[10.1002/grl.50274](https://doi.org/10.1002/grl.50274), 2013.

1045 Vinayachandran P. N., Yamagata, T.: Monsoon Response of the Sea around Sri Lanka:
1046 Generation of Thermal Domes and Anticyclonic Vortices, J. Phy. Oceano., 28, 1946 – 1960, doi:
1047 [10.1175/1520-0485.1998](https://doi.org/10.1175/1520-0485.1998).

1048 Vinayachandran, P. N., Chauhan, P., Mohan, M., Nayak, S.: Biological response of the sea
1049 around Sri Lanka to summer monsoon, Geophys. Res. Lett., 31, L01302,
1050 doi:[10.1029/2003GL018533](https://doi.org/10.1029/2003GL018533), 2004.

1051 Wang .X. J., Behrenfeld. M., Le Borgne .R., Murtugudde .R., and Boss. E.: Regulation of
1052 phytoplankton carbon to chlorophyll ratio by light, nutrients and temperature in the equatorial
1053 Pacific Ocean: a basin-scale model. *Biogeosciences.*, 6, 391 – 404, doi:10.5194/bg-6-391-2009,
1054 2009.

1055 Weiss, R. F.: Carbon dioxide in water and seawater: The solubility of a non-ideal gas, *Mar.*
1056 *Chem.*, 2, 203-215, 1974.

1057 Wiggert J. D., Jones. B. H., Dickey .T D., Brink .K. H., Weller .R .A., Marra. J., Codispoti. L.
1058 A.: The Northeast Monsoon's impact on mixing, phytoplankton biomass and nutrient cycling in
1059 the Arabian Sea, *Deep Sea Res. Pt. II*, 47, 1353-1385, [doi:10.1016/S0967-0645\(99\)00147-2](https://doi.org/10.1016/S0967-0645(99)00147-2),
1060 2000.

1061 Wiggert, J. D., Hood, R. R., Banse, K., Kindle, J. C.: Monsoon-driven biogeochemical processes
1062 in the Arabian Sea, *Progr. Oceanogr.*, 65, 176-213, [doi:10.1016/j.pocean.2005.03.008](https://doi.org/10.1016/j.pocean.2005.03.008), 2005.

1063 Wiggert. J. D., Murtugudde, R. G., Christian J. R.: Annual ecosystem variability in the tropical
1064 Indian Ocean: results of a coupled bio-physical ocean general circulation model, *Deep Sea Res.*
1065 *Pt. II.*, 53, 644-676, doi:10.1016/j.dsr2.2006.01.027, 2006.

1066 Xie, S. P., Annamalai, H., Schott, F. A., McCreary Jr. J. P.: Structure and mechanism of south
1067 Indian ocean climate variability, *J. clim.*, 15, 864 – 878, doi: [10.1175/1520-0442](https://doi.org/10.1175/1520-0442.2002), 2002.

1068 Xing W., Xiaomei. L., Haigang Z., Hailong. L.: Estimates of potential new production in the
1069 Java-Sumatra upwelling system, *Chinese Journal of Oceanology and Limnology.*, 30, 1063-
1070 1067, doi:10.1007/s00343-012-1281, 2012.

1071 Yamanaka, Y., Yoshie, N, Masahiko Fujii, Maka .N. Aita and Kishi. M. J.: An Ecosystem
1072 coupled with Nitrogen-Silicon-Carbon cycles applied to station A7 in the Northwestern Pacific,
1073 J. of Oceanogr., 60, p227-241, doi: 10.1023/B:JOCE.0000038329.91976.7d, 2004.

1074 Zhou X., Weng. E., Luo., Y.: Modelling patterns of nonlinearity in the ecosystem responses to
1075 temperature, CO₂ and precipitation changes, Eco. Appli., 18, 453 – 466, doi: 10.1890/07-0626.1,
1076 2008.

1077

1078

Table: 1 WAS = Western Arabian Sea, SLD = Sri Lanka Dome, SC = Sumatra Coast, SCTR = Seychelles-Chagos Thermocline Ridge. JJAS mean and the climatological annual mean of CO₂ flux from Takahashi observations, constZc, and varZc simulations. Units are mol m⁻² yr⁻¹.

Regions	CO ₂ flux (mol m ⁻² yr ⁻¹)					
	JJAS Mean			Annual Mean		
	OBS	constZc	varZc	OBS	constZc	varZc
WAS	1.99	1.44 ± 0.2	2.31 ± 0.4	0.94	0.80 ± 0.1	1.07 ± 0.2
SLD	1.79	-0.008 ± 0.2	0.24 ± 0.09	0.8	-0.02 ± 0.1	0.10 ± 0.2
SC	0.31	0.60 ± 0.5	1.51 ± 1.01	0.21	0.21 ± 0.3	0.53 ± 0.5
SCTR	0.82	-0.32 ± 0.3	-0.05 ± 0.4	0.55	-0.02 ± 0.1	-0.07 ± 0.2

Table: 2 Same as Table 1, but for pCO₂. Units are µatm.

Regions	pCO ₂ (µatm)					
	JJAS Mean			Annual Mean		
	OBS	constZc	varZc	OBS	constZc	varZc
WAS	397.58	389.18 ± 3.7	399.95 ± 5.01	394.69	389.62 ± 3.9	391.19 ± 4.7
SLD	382.44	371.67 ± 6.04	379.24 ± 8.9	380.21	370.76 ± 6.1	374.94 ± 9.6
SC	372.52	382.36 ± 12.7	402.14 ± 21.8	372.69	374.65 ± 9.3	381.76 ± 13.6
SCTR	377.18	365.71 ± 5.08	370.72 ± 7.4	379.89	372.69 ± 4.7	369.00 ± 5.4

Table: 3 JJAS mean and the climatological annual mean of export production from satellite-derived Net Primary Production data, constZc, and varZc simulations. Units are $\text{g C m}^{-2} \text{yr}^{-1}$.

Regions	Export Production ($\text{g C m}^{-2} \text{yr}^{-1}$)					
	JJAS Mean			Annual Mean		
	OBS	constZc	varZc	OBS	constZc	varZc
WAS	123.57	84.81 ± 16.04	147.19 ± 23.8	94.31	77.41 ± 15.1	122.54 ± 25.2
SLD	51.54	167.71 ± 59.04	151.51 ± 46.4	43.25	144.43 ± 49.8	156.08 ± 43.8
SC	58.87	260.11 ± 104.7	310.03 ± 99.5	54.53	172.52 ± 72.4	215.52 ± 70.8
SCTR	51.08	57.39 ± 14.2	99.23 ± 21.8	40.45	55.15 ± 17.9	80.35 ± 26.04

Table: 4 Model derived values for New production. Units are $\text{g C m}^{-2} \text{yr}^{-1}$.

Regions	New Production ($\text{g C m}^{-2} \text{yr}^{-1}$)					
	JJAS Mean			Annual Mean		
	OBS	constZc	varZc	OBS	constZc	varZc
WAS	--	150.84 ± 27.9	133.03 ± 19.5	--	108.43 ± 23.4	81.47 ± 15.7
SLD	--	141.93 ± 64.1	77.78 ± 27.6	--	111.05 ± 71.1	50.37 ± 26.3
SC	--	63.64 ± 30.9	78.11 ± 29.1	--	56.69 ± 43.3	54.58 ± 23.3
SCTR	--	12.17 ± 16.3	13.32 ± 18.6	--	13.74 ± 15.5	12.94 ± 13

Table 5: Biological pump impact over DIC in the model due to constZc and varZc simulations for JJAS and annual mean.

Regions	Biological Pump ($\text{g C m}^{-2} \text{ yr}^{-1}$)			
	constZc		varZc	
	JJAS Mean	Annual Mean	JJAS Mean	Annual Mean
WAS	45.18 ± 14.8	45.49 ± 14.38	151.7 ± 23.8	126.67 ± 24.3
SLD	89.39 ± 58.1	108.65 ± 48.6	156.07 ± 48.4	161.15 ± 43.5
SC	235.54 ± 95.4	155.21 ± 67.4	319.16 ± 94.9	222.92 ± 68.7
SCTR	30.49 ± 13.4	26.81 ± 16.8	103.13 ± 19.6	83.98 ± 23.6

Table 6: Same as Table 5, But for Solubility pump.

Regions	Solubility Pump ($\text{g C m}^{-2} \text{ yr}^{-1}$)			
	constZc		varZc	
	JJAS Mean	Annual Mean	JJAS Mean	Annual Mean
WAS	17.29 ± 3.5	9.63 ± 2.1	27.72 ± 4.8	12.92 ± 2.7
SLD	-0.09 ± 2.4	-0.32 ± 2.3	2.9 ± 3.5	1.31 ± 3.5
SC	7.22 ± 6.9	2.56 ± 3.8	18.17 ± 12.1	6.43 ± 6.0
SCTR	-3.95 ± 3.7	-0.35 ± 2.3	-0.61 ± 5.3	-0.86 ± 2.8

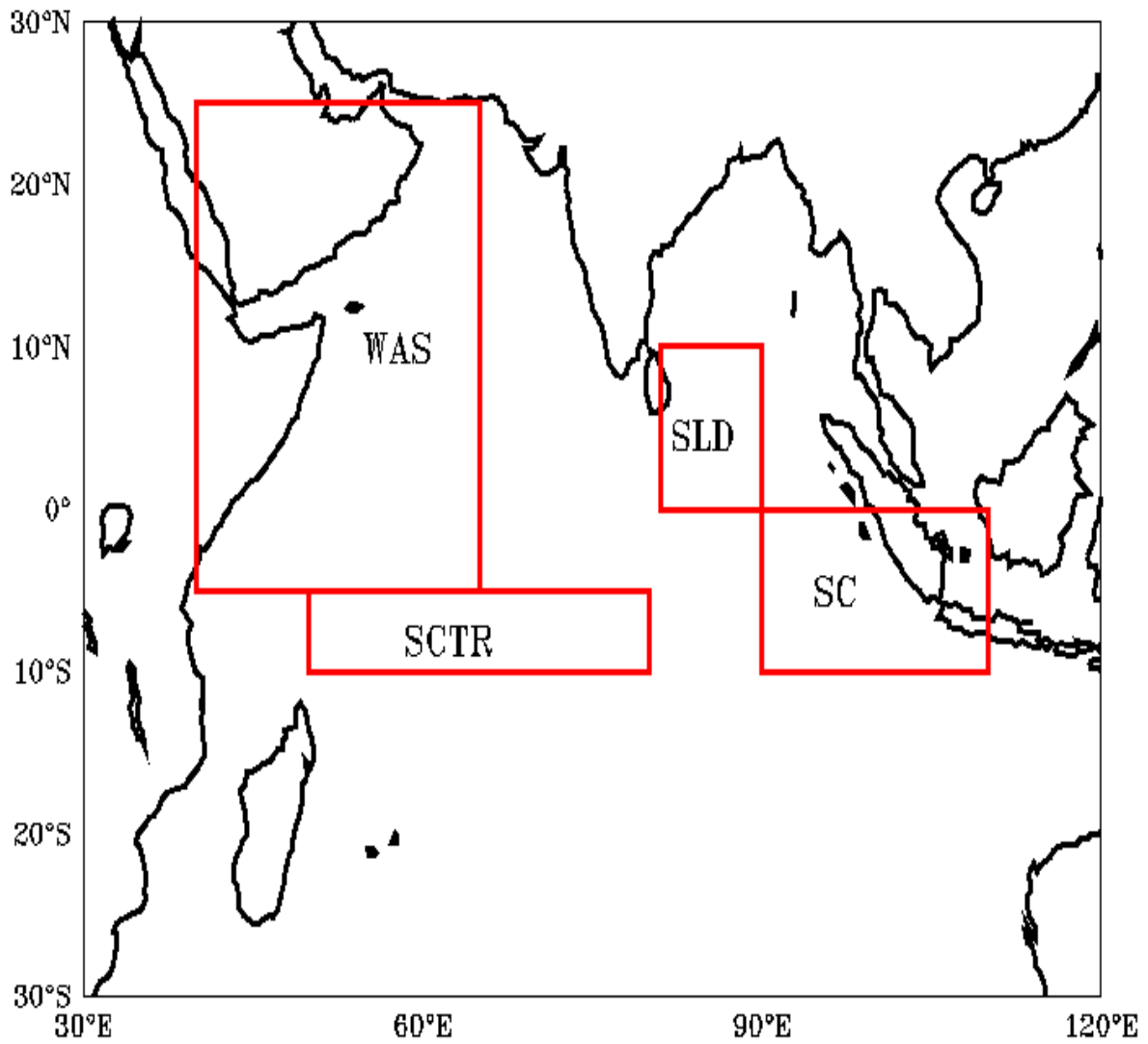


Figure 1: Red boxes shows the study regions (1) WAS (Western Arabian Sea, 40°E:65°E, 5°S:25°N) (2) SLD (Sri Lanka Dome, 81°E:90°E, 0°:10°N) (3) SCTR (Seychelles-Chagos Thermocline Ridge, 50°E:80°E, 5°S:10°S) and (4) SC (Sumatra Coast, 90°E:110°E, 0°:10°S).

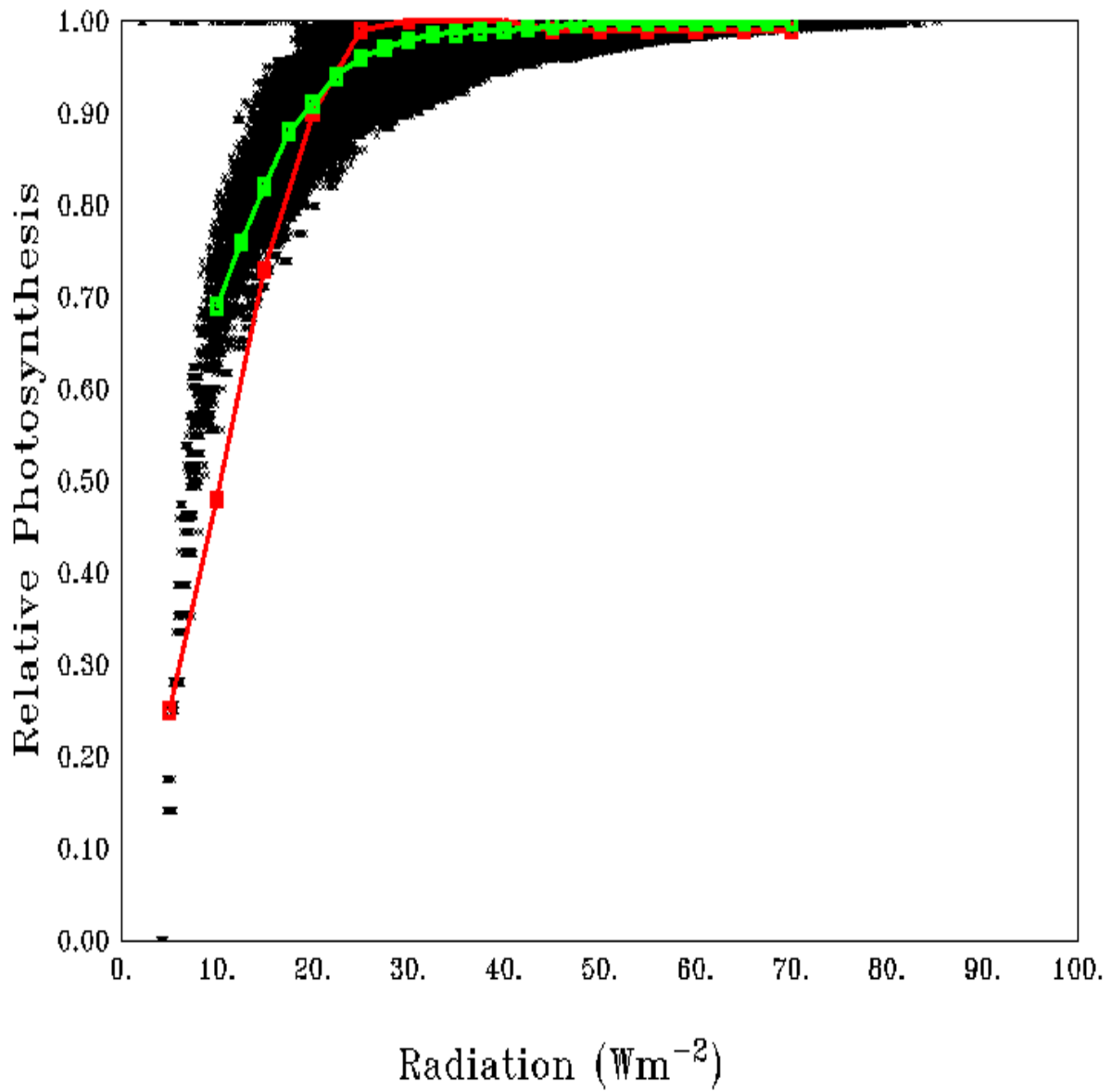


Figure 2: Scatter of average relative photosynthesis versus different light intensities in the model (black dots) and its mean (green curve). The red curve shows the theoretical P – I curve from Parsons et al., (1984).

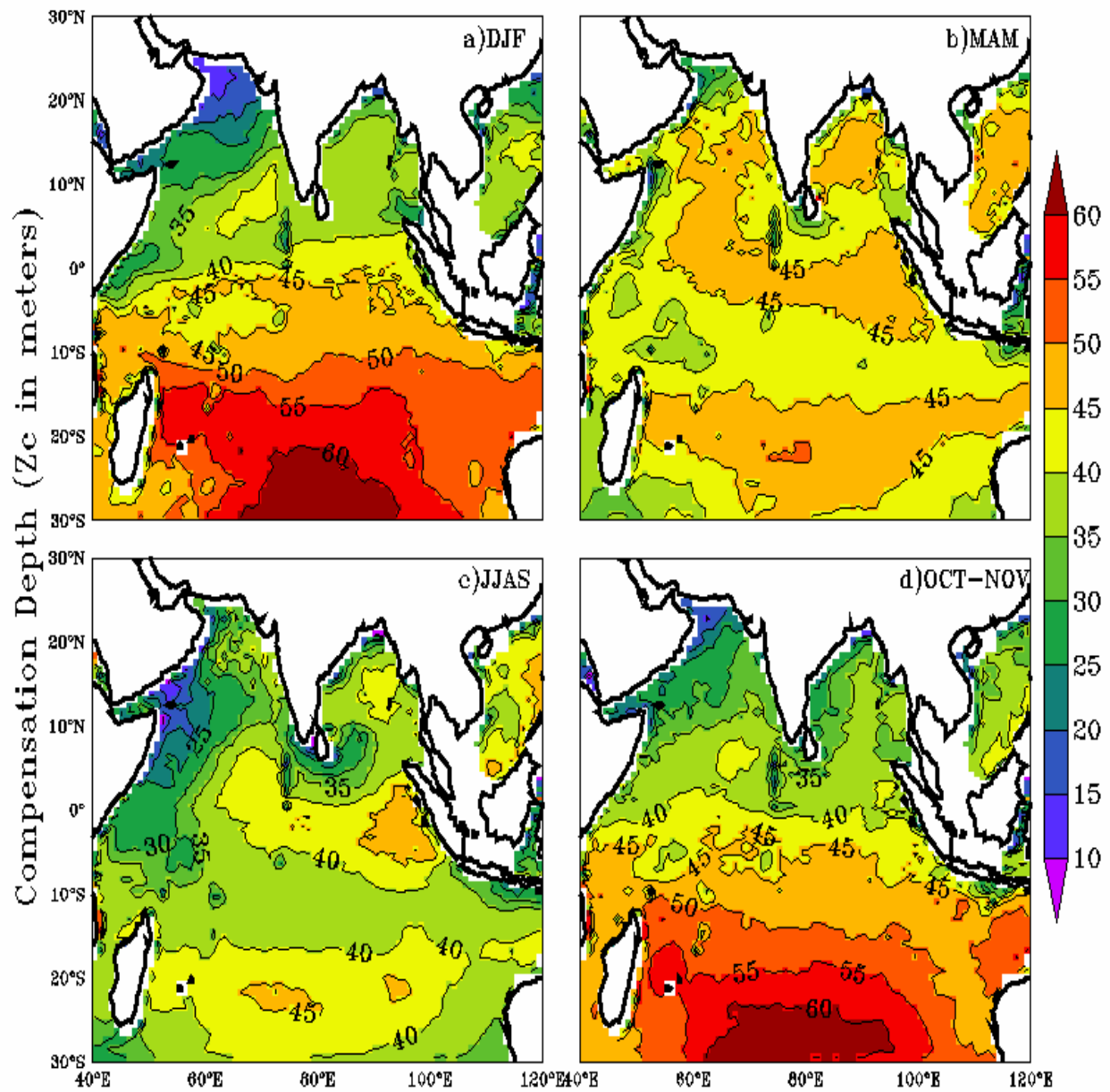


Figure 3: Seasonal-mean maps of varying compensation depth ($\text{var}Z_c$), (a) December to February (DJF), (b) March to May (MAM), (c) June to September (JJAS), (d) October to November (OCT-NOV). Units are meters.

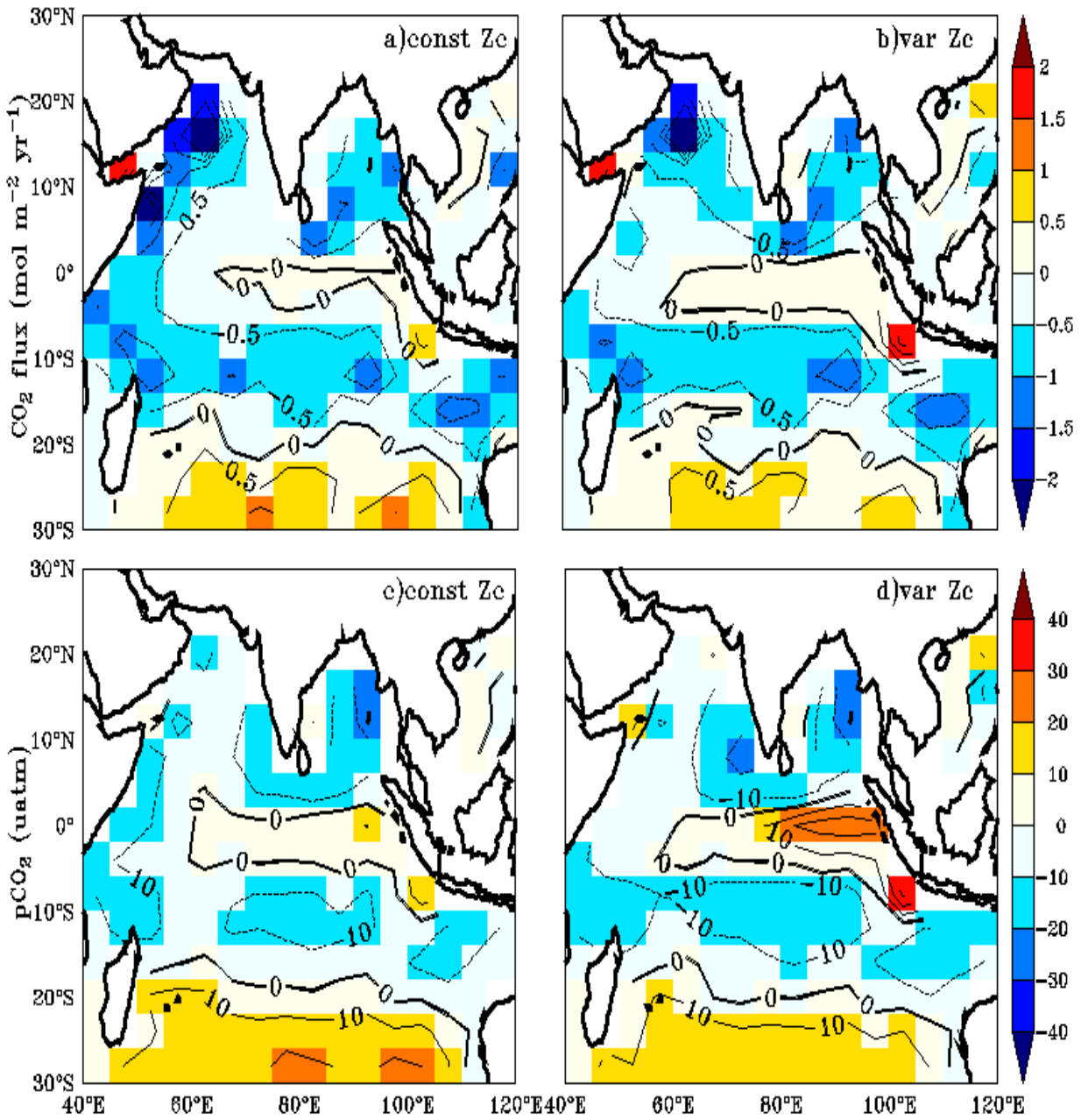


Figure 4: Annual mean biases in the model evaluated against Takahashi et al. (2009) observations for CO₂ flux (a, b) and pCO₂ (c, d) with constant Zc (constZc) and varying Zc (varZc). Units of CO₂ flux and pCO₂ are mol m⁻² yr⁻¹ and μatm, respectively.

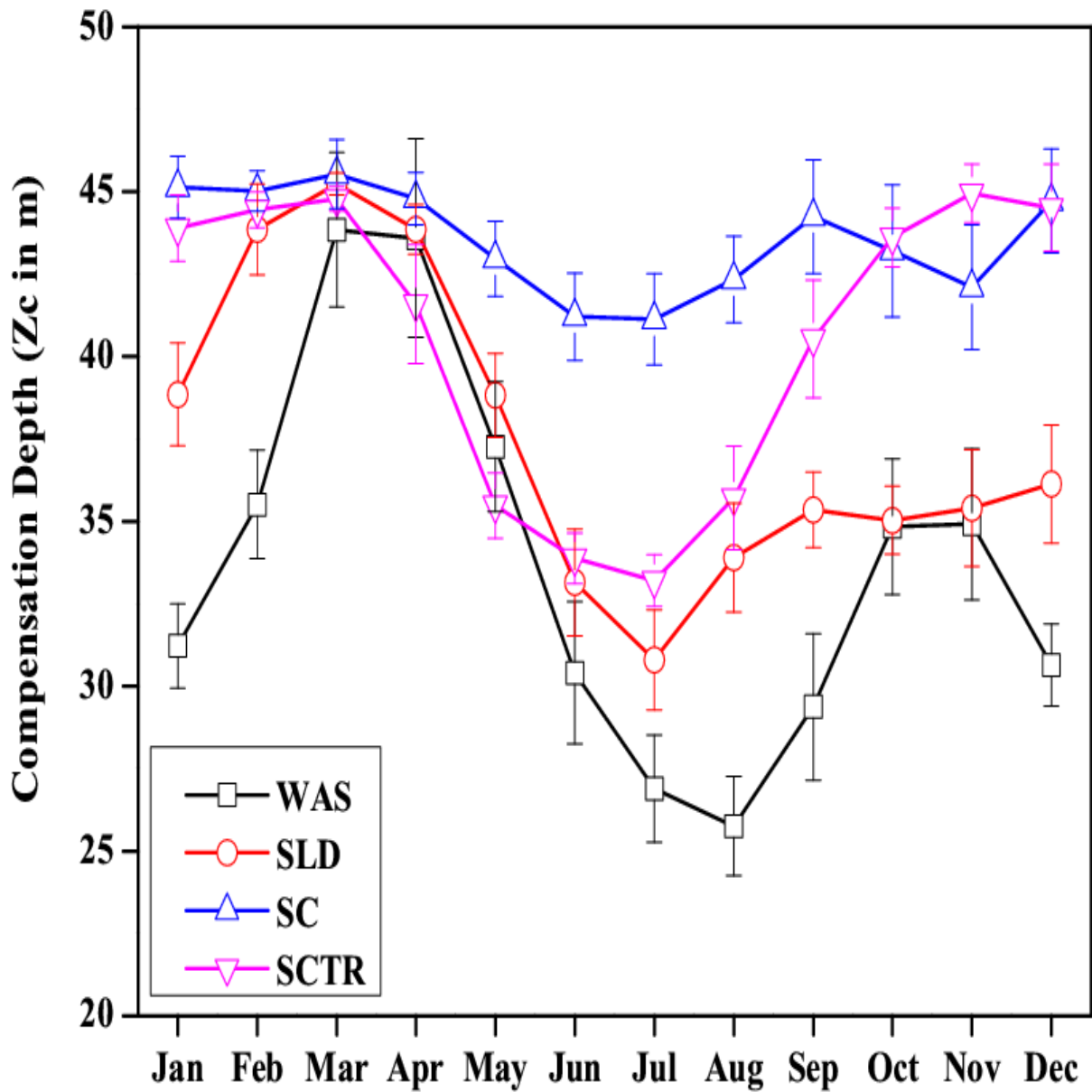


Figure 5: Seasonal variations in varZc over the study regions shown as climatology computed over 1990-2010. Error bar shows standard deviations of individual months over these years. Units are meters.

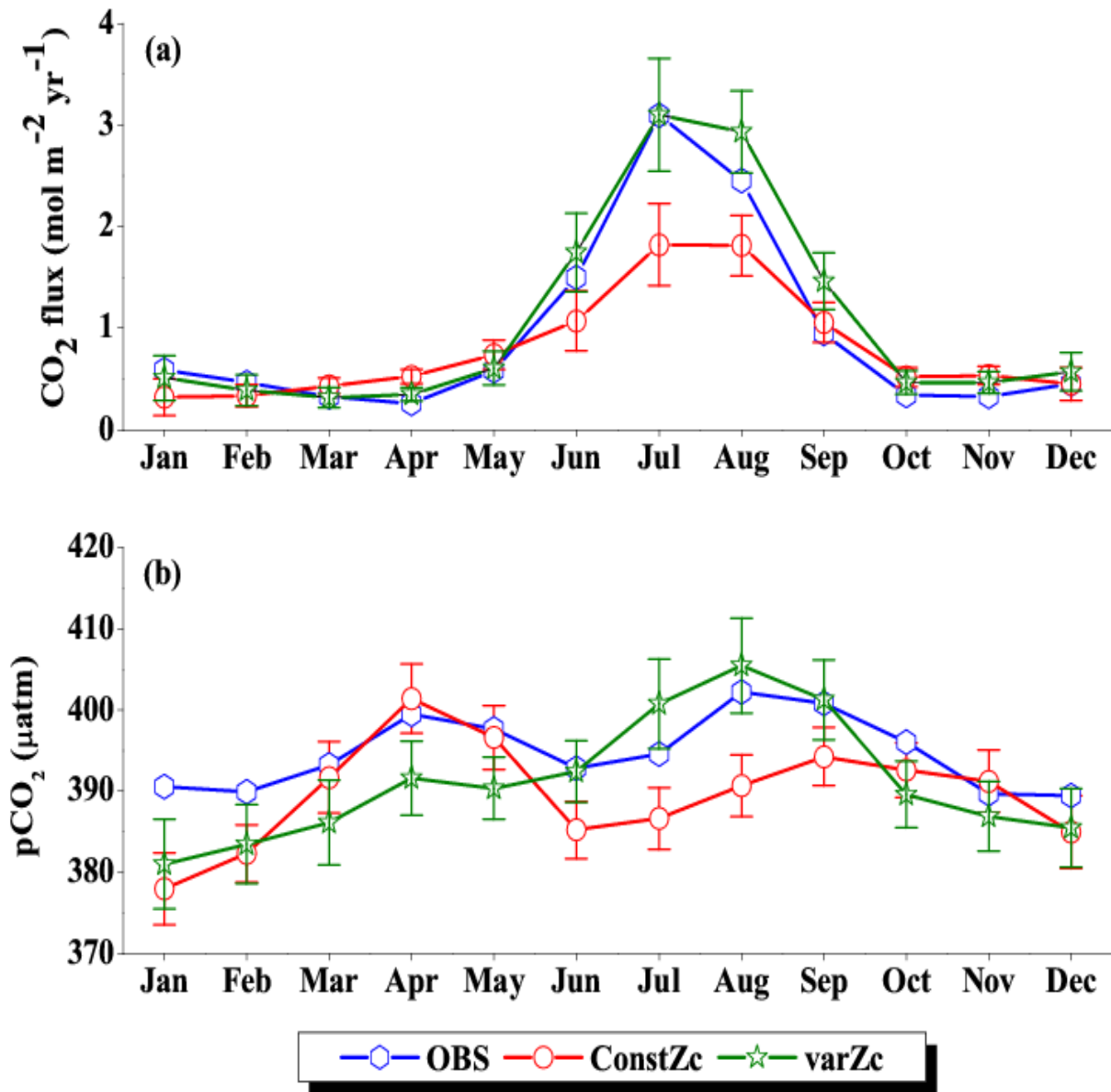


Figure 6: Comparison of model (a) CO₂ flux and (b) pCO₂ simulated with constZc and varZc with that of Takahashi et al. (2009) observations (OBS) over WAS as climatology computed over 1990-2010. Error bar shows standard deviations of individual months over these years. Units of CO₂ flux and pCO₂ are mol m⁻² yr⁻¹ and µatm, respectively. Legend is common for both graphs.

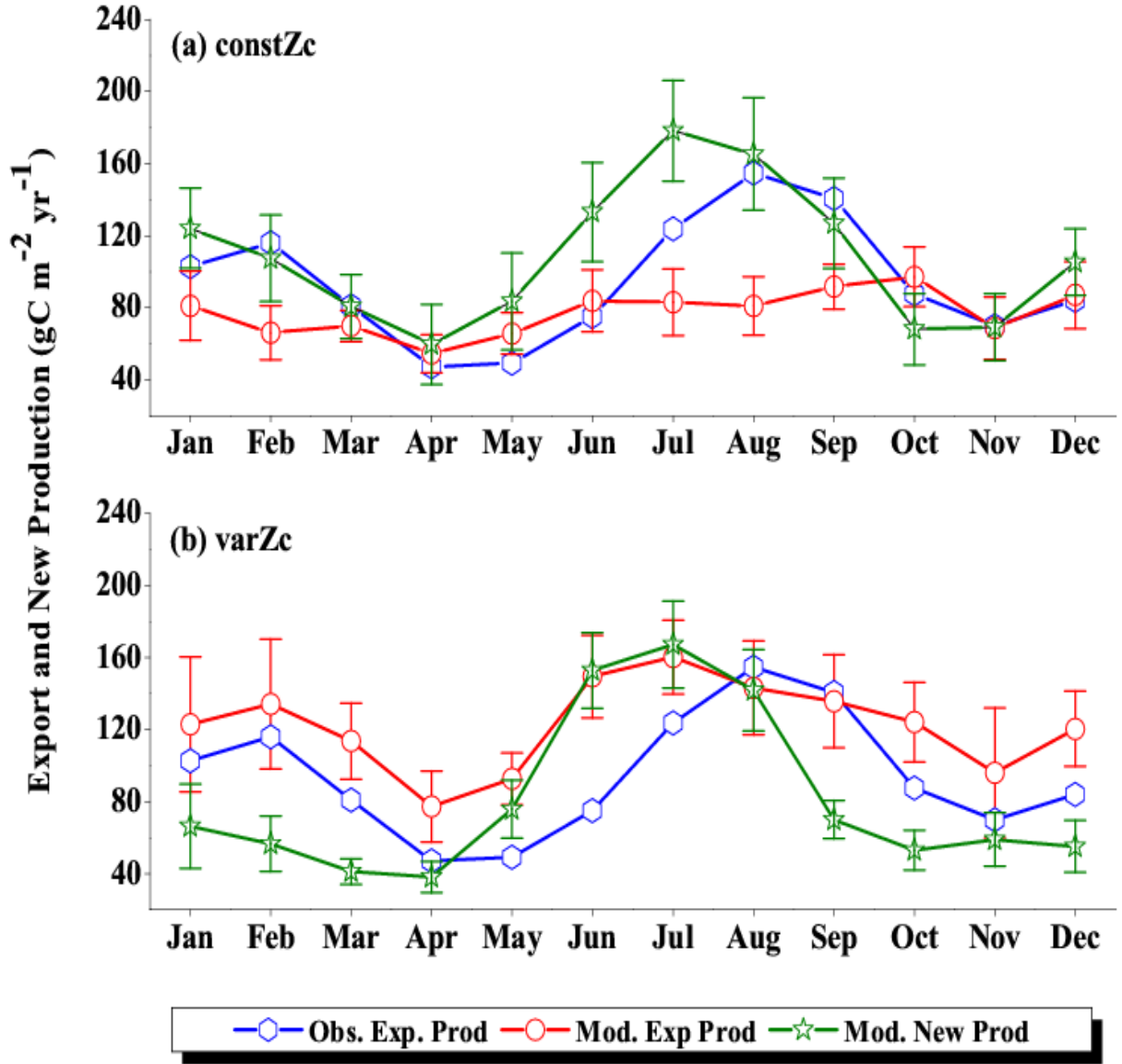


Figure 7: Comparison of model export production (Mod. Exp. Prod) and new production (Mod. New Prod) with satellite-derived export production (Obs. Exp. Prod) for (a) ConstZc and (b) varZc simulations for WAS. Units are $\text{g C m}^{-2} \text{ yr}^{-1}$. Legends are common for both graphs.

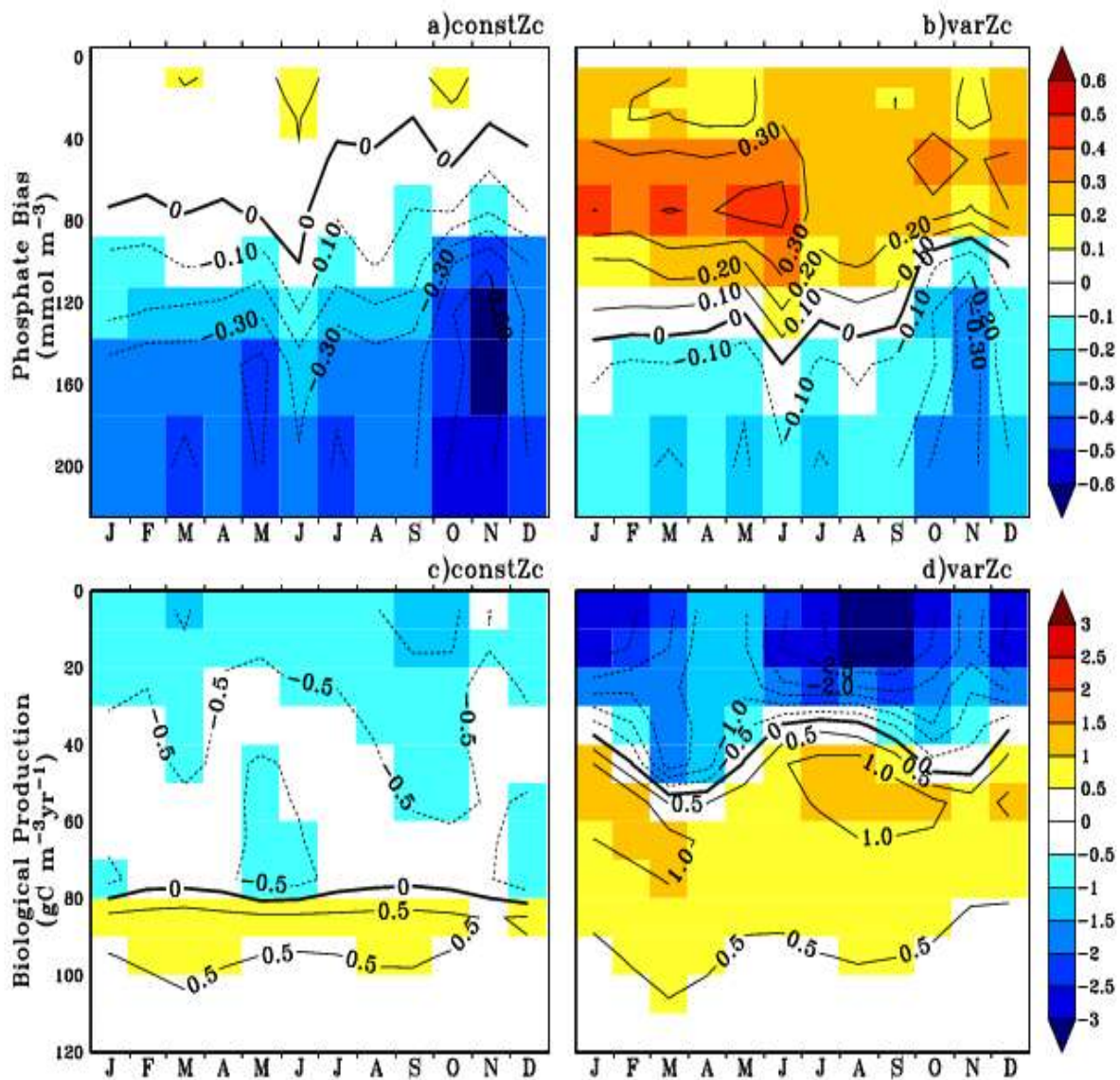


Figure 8: Annual mean bias of model phosphate when compared with climatological observational data (a) for constZc and (b) for varZc simulations. Corresponding annual mean biological source/sink profiles (c, d) in the model for WAS. Unit of phosphate is mmol m^{-3} and biological source/sink is $\text{g C m}^{-3}\text{yr}^{-1}$.

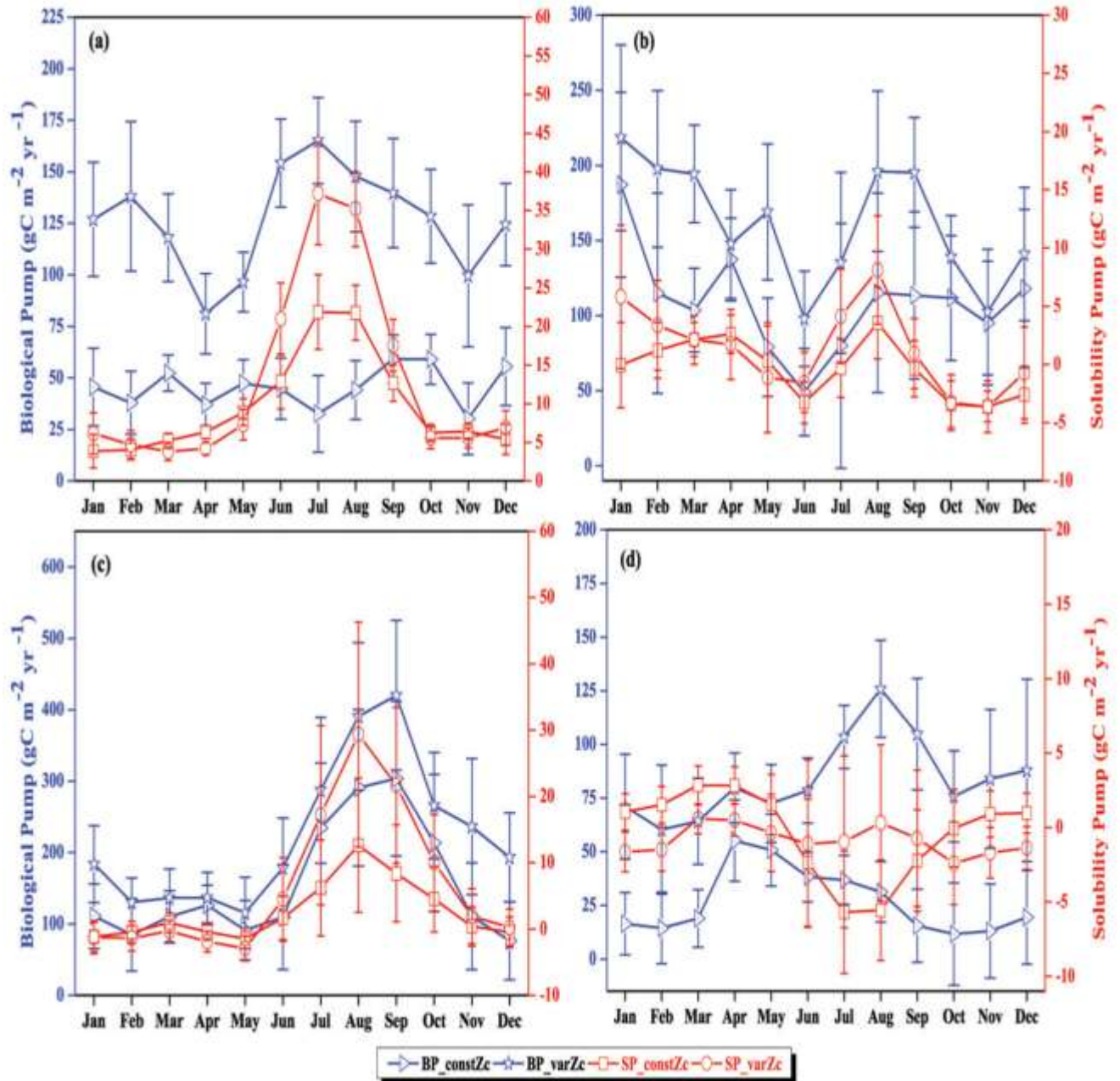


Figure 9: The strength of the biological pump (BP, black lines) and solubility pump (SP, red lines) from constZc and varZc simulations for (a) WAS (b) SLD (c) SC and (d) SCTR. The left axis shows the biological pump and the right axis shows the solubility pump. Error bar shows standard deviations of individual months over the years 1990 - 2010. Units are $\text{g C m}^{-2} \text{ yr}^{-1}$.

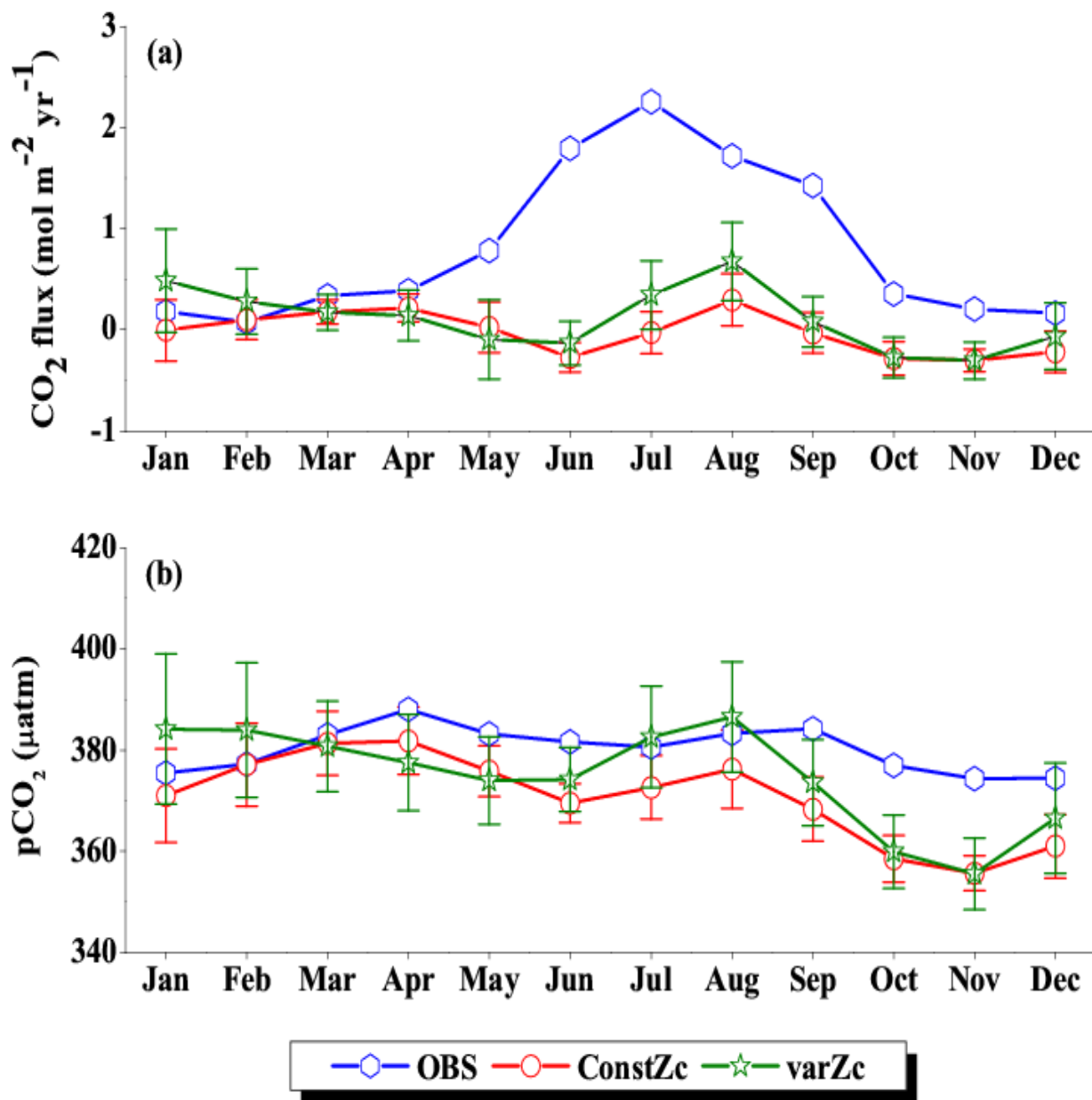


Figure 10: Same as Figure (6), but for SLD.

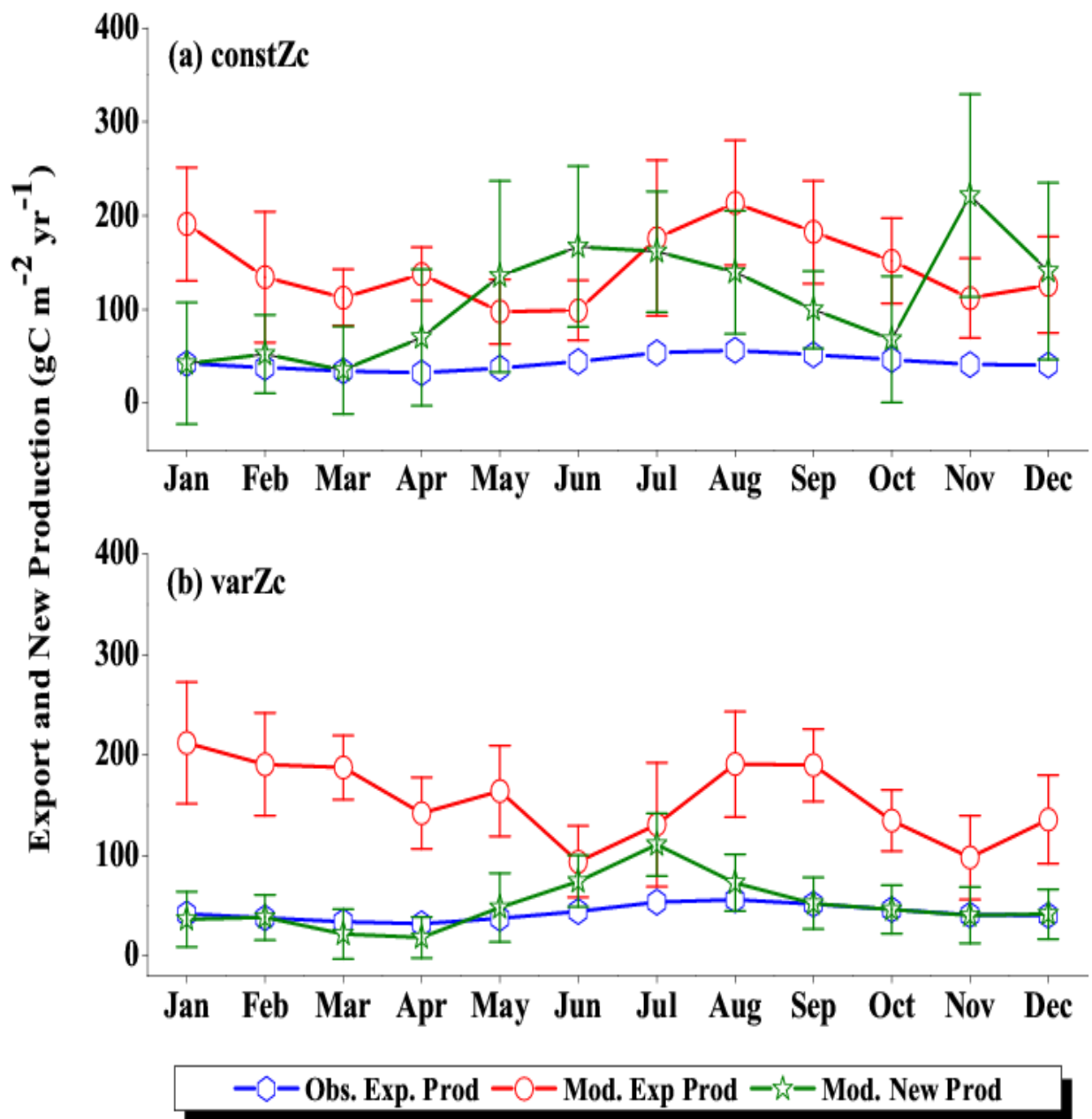


Figure 11: Same as Figure (7), but for SLD.

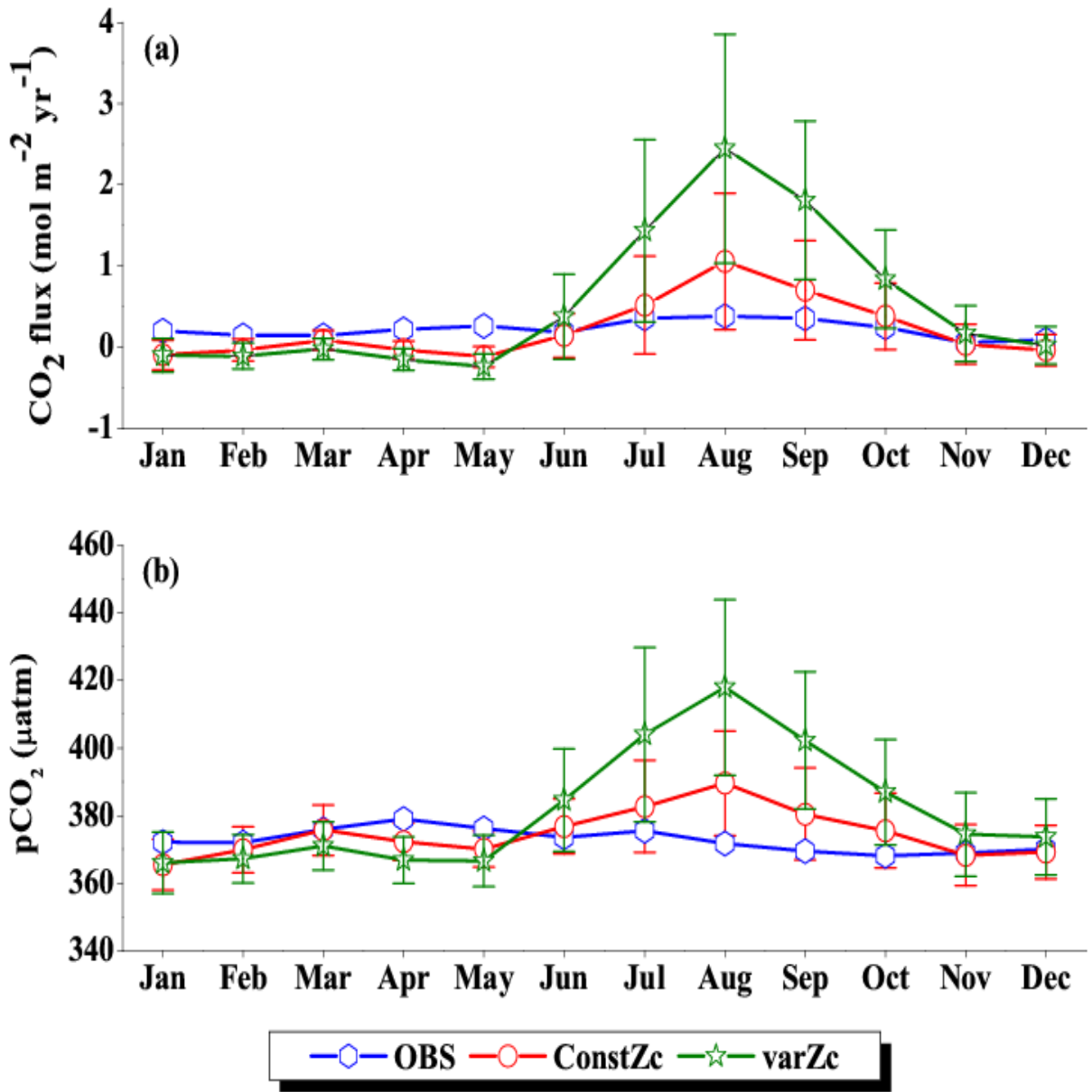


Figure 12: Same as Figure (6), but for SC.

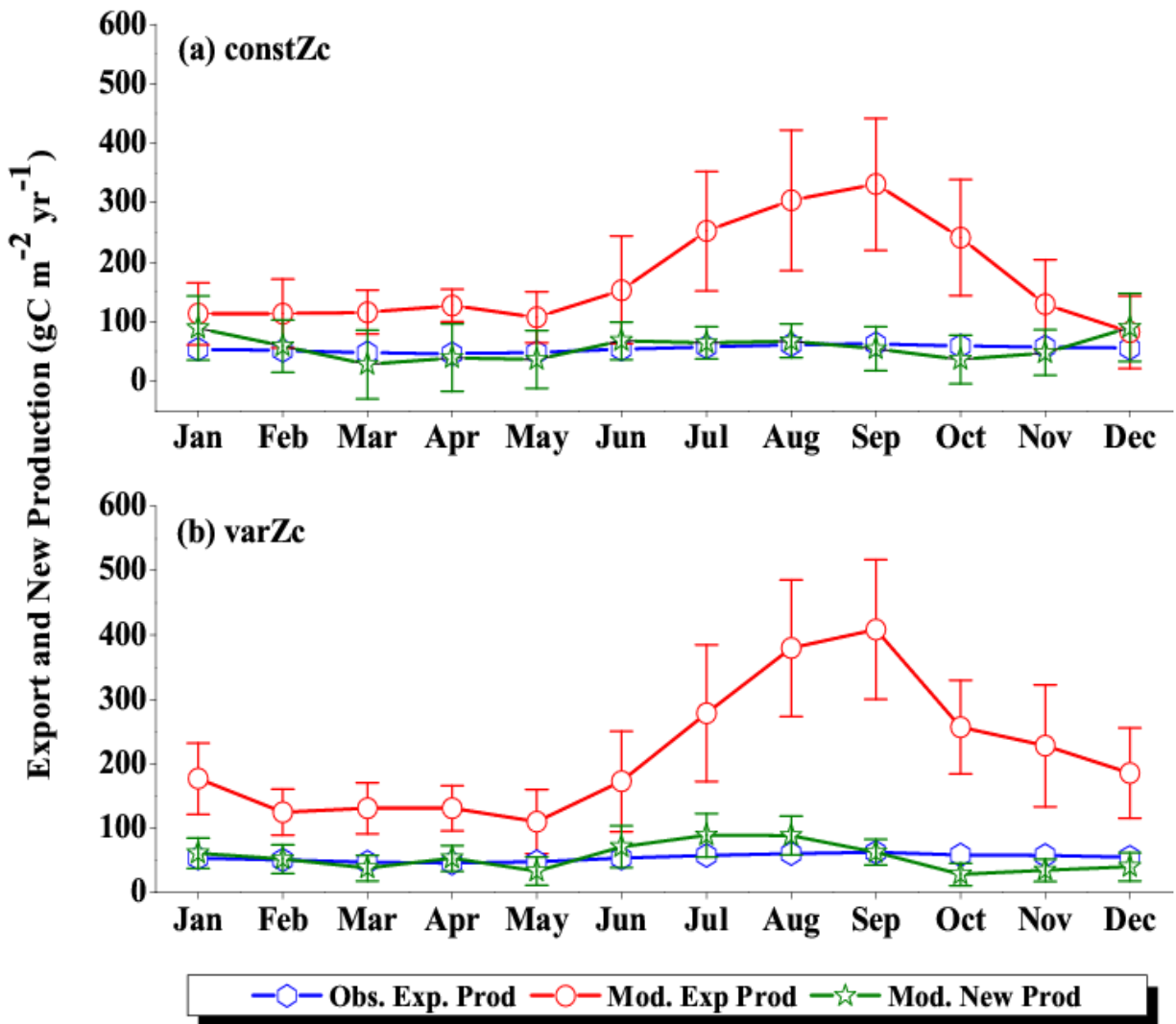


Figure 13: Same as Figure (7), but for SC.

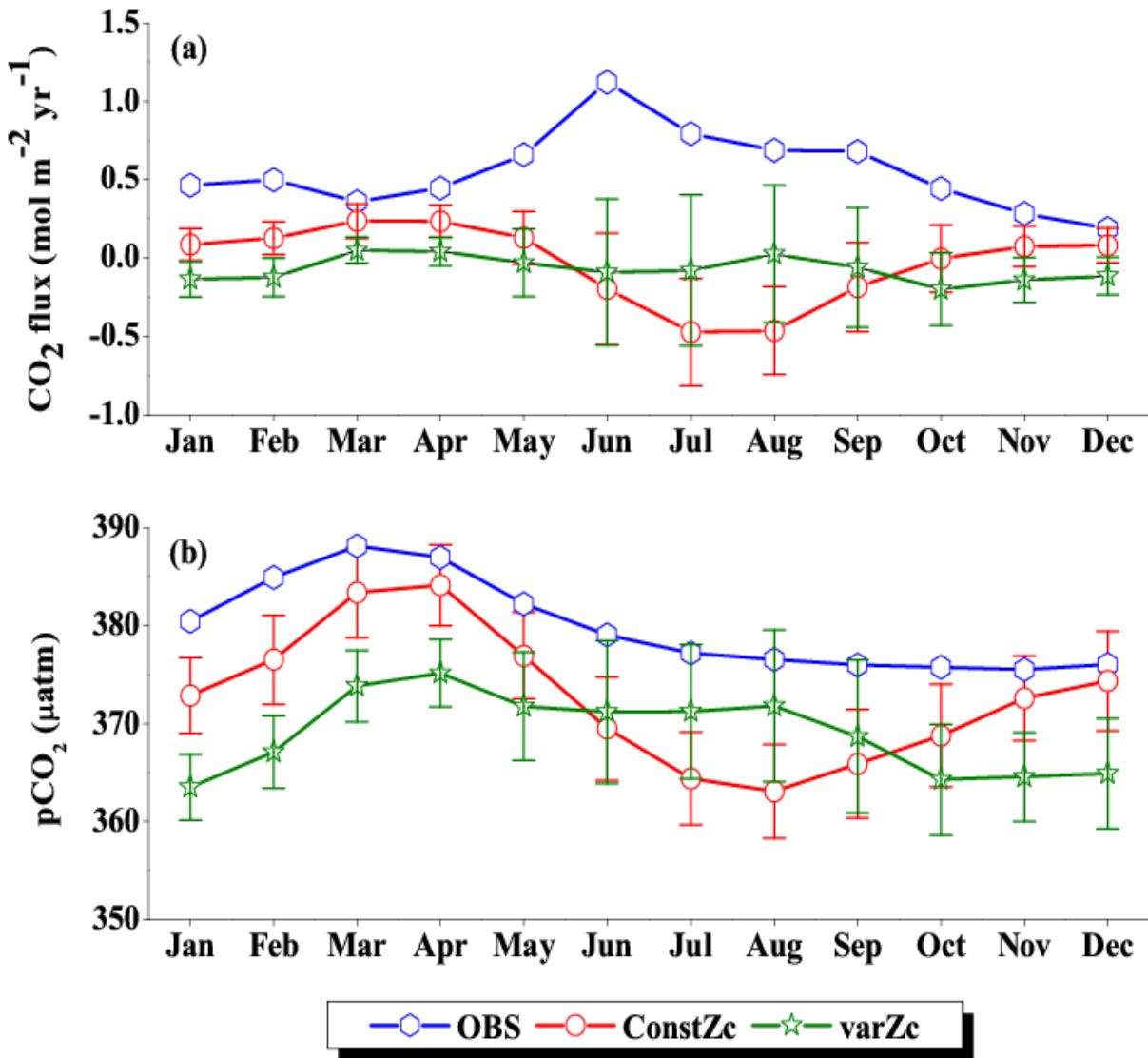


Figure 14: Same as Figure (6), but for SCTR.

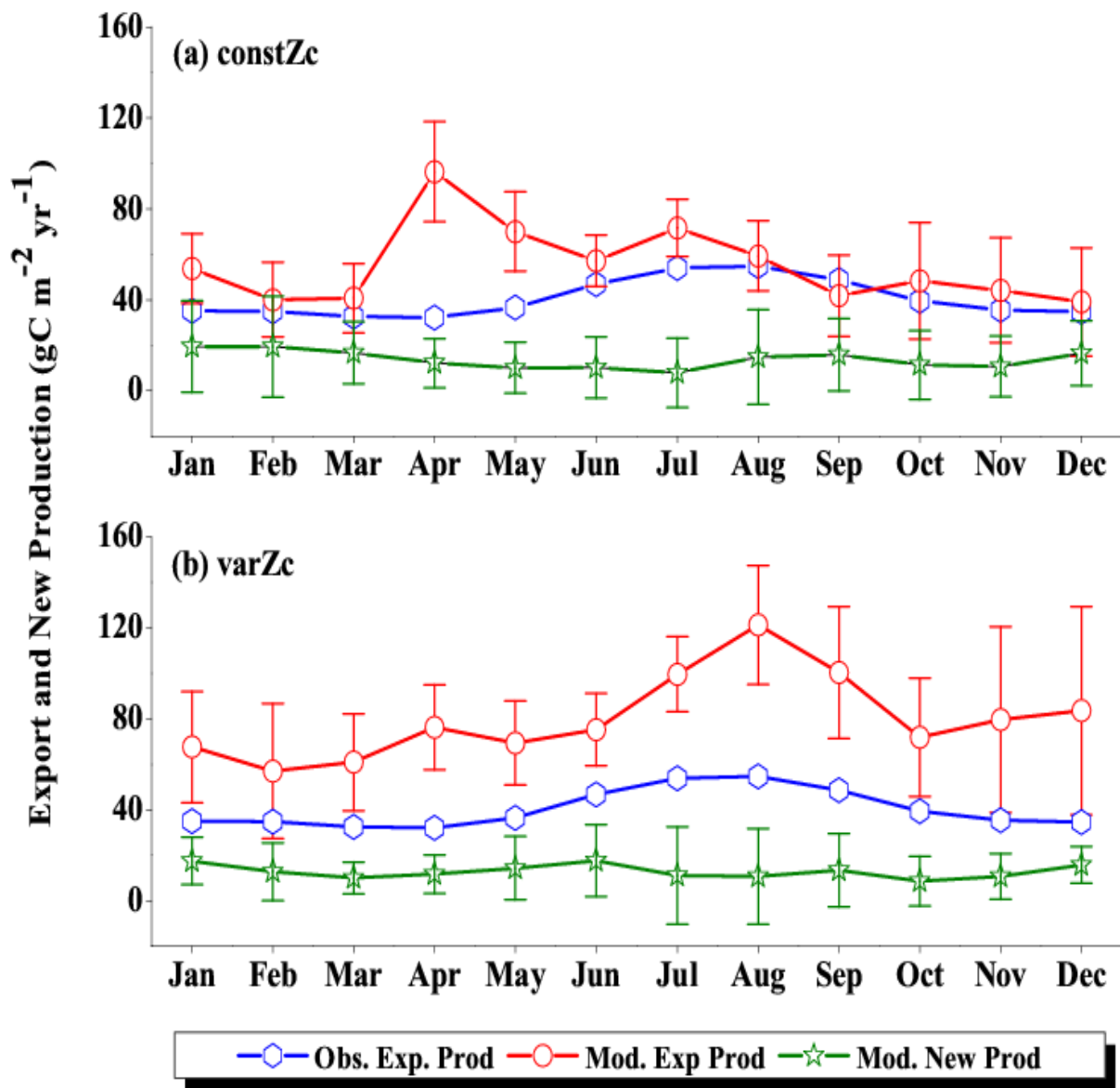


Figure 15: Same as Figure (7), but for SCTR.